Timed mesodermal FGF and BMP govern the multi-step thyroid specification

Benoit Haerlingen[1], Robert Opitz[2], Isabelle Vandernoot[1,3], Angelo Molinaro[4], Meghna Shankar[1], Pierre Gillotay[1], Achim Trubiroha[5] and Sabine Costagliola[1].

Authors' Affiliations

[1] Institute of Interdisciplinary Research in Molecular Human Biology (IRIBHM), Université Libre de Bruxelles, 1070 Brussels, Belgium

[2] Institute of Experimental Pediatric Endocrinology, Charité Universitätsmedizin, 13353 Berlin, Germany

[3] Hopital Erasme, Genetic Department, Université Libre de Bruxelles, 1070 Brussels, Belgium

[4] Department of experimental and clinical medicine, endocrinology unit, university of Pisa, Italy

[5] Department Chemicals and Product Safety, German Federal Institute for Risk Assessment (BfR), 10609 Berlin, Germany

Correspondence

Sabine Costagliola: scostag@ulb.ac.be

Summary

The thyroid plays an essential role in homeostasis and development, but the extrinsic regulation of its embryonic development remains poorly understood. Recently, we have identified the FGF and BMP pathways to be crucial for thyroid specification and have confirmed the hypothesis that the cardiac mesoderm provides the FGF and BMP ligands to regulate this process. However, it is not clear how these ligands control thyroid specification. To study the molecular mechanisms underlying early thyroid development, we combined a pharmacological approach in zebrafish embryos with genetic models, to modulate the activity of the FGF and BMP pathways at different embryonic stages. We first characterized the expression of the transcription factors pax2a and nkx2.4b - the two main early thyroid markers - in the anterior foregut endoderm and observed that pax2a was expressed from 18 hours post fertilization (hpf) and marked a large endodermal cell population while nkx2.4b was expressed from 24 hpf and marked only a subset of the pax2a-positive endodermal cells. Interestingly, the activity profiles of FGF and BMP coincided with the detection of pax2a and nkx2.4b expression, respectively. Brief modulations of the FGF and/or

BMP pathways support the hypothesis that the FGF pathway regulates the expression of pax2a and the BMP pathway regulates the expression of nkx2.4b. Furthermore, inhibition of the BMP pathway during early segmentation has dramatic effects on thyroid specification, probably via the FGF pathway. Together with our previous observations, we propose here, an updated model of early thyroid development in which the foregut endoderm receives several synchronized waves of FGF and BMP signals from the cardiac mesoderm, which result in sequential activation of pax2a and nkx2.4b gene expression and subsequent thyroid specification.

Keywords

Zebrafish, endoderm, thyroid, specification, FGF, BMP

Introduction

The thyroid is an essential hormone-secreting gland present in all vertebrates. It regulates through the production of thyroid hormones (TH) key processes in adult homeostasis as well as embryonic development (Bernal, 2007; Buchholz et al., 2006; Mullur et al., 2014). The functional unit of the thyroid or the follicle, consists of a single-layer epithelium of thyroid follicular cells (TFCs) and its primary functions are to synthesize, store and secrete THs. In newborns, the inability to synthesize sufficient amount of TH causes congenital hypothyroidism (CH) and accounts for approximately 80-85% of the patients with thyroid dysgenesis (TD). (Corbetta et al., 2009; Wassner, 2018). To date, monogenic mutations have been linked to CH in fewer than 5% of the patients (Wassner, 2018). Despite the unknown genetic origin, CH patients present associated malformations and 55% of these malformations affect the heart or the main blood vessels (Olivieri et al., 2002), thus suggesting a possible correlation between the two developmental defects.

The first event in thyroid organogenesis, is the specification of the thyroid progenitors in the anterior most domain of the foregut at embryonic day (E) 8.5 and at 24 hours post fertilization (hpf) in mouse and zebrafish, respectively (Kimura, 1996; Rohr and Concha, 2000). The thyroid progenitors are characterized by the co-expression of *Nkx2.1* (*nkx2.4b* in zebrafish) and *Pax8* (*pax2a* in zebrafish) (Kimura et al., 1996; Mansouri et al., 1998; Wendl et al., 2002). Therefore, the initiation of the expression of these two markers, alongside with that of *Hhex* and *Foxe1* (Thomas et al., 1998; Zannini et al., 1997), defines the thyroid specification. Next, the progenitors undergo a complex series of morphogenetic events including budding, migration and folliculogenesis to complete thyroid development (Alt et al., 2006; Fagman et al., 2006; Opitz et al., 2012). During these events, they start to express functional differentiation genes such as the

thyroglobulin (*Tg*), thyroid peroxidase (*Tpo*) or the sodium-iodide symporter (*Slc5a5*, previously known as *Nis*) (Fagman and Nilsson, 2011; Opitz et al., 2011).

Surprisingly, relatively little is known about the extrinsic regulation of thyroid organogenesis. Mutant mice with defective fibroblast growth factor (FGF) signaling pathway gave the first clues that FGF regulates thyroid development as the mice show severely hypoplasic or no thyroid at all (Celli et al., 1998; Ohuchi et al., 2000; Revest et al., 2001). The functions of FGF in thyroid development have been confirmed *in vitro* and *in vivo* in several species (Haerlingen et al., 2019; Kurmann et al., 2015; Longmire et al., 2012; Serls et al., 2005; Wendl et al., 2007): FGF inhibition always prevents thyroid progenitors from specifying and the *in vitro* morphogens-based protocols use recombinant FGF2 ligands to induce thyroid specification from anterior foregut endoderm. Interestingly, it has been shown that the bone morphogenetic protein (BMP) signaling pathway is crucial too, as inhibition of this pathway blocks thyroid specification *in vivo* and *in vitro. So* thyroid differentiation requires the combination of the FGF2 and BMP4 ligands (Kurmann et al., 2015). Furthermore, we recently performed a small molecule screen to identify the signaling pathways regulating early thyroid development in zebrafish (Haerlingen et al., 2019) and identified the FGF and BMP pathways as the most important for thyroid specification, thus confirming their roles in early thyroid development (Kurmann et al., 2015; Wendl et al., 2007). Among the tested morphogen signaling pathways, we found no other to be essential for thyroid progenitor specification (Haerlingen et al., 2019).

Presently, the cardiac mesoderm is believed to be the source of the required FGF and BMP ligands (Serls et al., 2005; Vandernoot et al., 2019; Wendl et al., 2007). Fate mapping analysis in zebrafish embryos revealed that the thyroid progenitors arise from a portion of the foregut endoderm that lies right above the anterior lateral plate mesoderm (aLPM) — the mesoderm domain that will give rise to the (Fagman et al., 2006; Wendl et al., 2007). In a recent report, we disrupted cardiac differentiation in zebrafish embryos and showed that thyroid specification was affected proportionally. Moreover, over-activation of BMP in heart-ablated embryos rescued thyroid progenitor specification, thus confirming that the cardiac mesoderm produces the required BMP ligands (Vandernoot et al., 2019). Such mesoderm-endoderm interactions have been shown to be crucial in other endoderm-derived organs (Gordillo et al., 2015; Herriges and Morrisey, 2014; Spagnoli, 2007). During lung development, a reciprocal communication between the aLPM and the foregut endoderm, which involves the retinoic acid, hedgehog, Wnt and BMP pathways, regulate *Sox2* and *Nkx2.1* in the endoderm and eventually results in lung fate induction (Rankin et al., 2016; 2018; Trisno et al., 2018).

Here, we have addressed the roles of the interactions between the cardiac mesoderm and the anterior foregut endoderm, mediated by FGF and BMP, in the context of the thyroid specification in zebrafish embryos. In particular, we have paid attention to the rapid temporal dynamics of the FGF and BMP morphogens and the differential response they trigger in the foregut endoderm. Our results indicate that the cardiac mesoderm governs the early thyroid development through FGF and BMP signaling at several time points. The FGF morphogen signaling pathway seems to play a single but prolonged role in thyroid specification, starting from 18/19 hpf. In contrast, the BMP morphogen signaling pathways seems to act two times sequentially: First, during early segmentation stages (10-13 hpf) and second, during thyroid specification itself (22/24 hpf). Our data also show that unlike what is currently described in the literature, the *pax2a* expression is initiated much earlier than that of *nkx2.4b* and marks a much larger endodermal cell population, thus defining a new, intermediate cell population. Based on these results as well as our previous studies, we propose an updated model of thyroid specification, which highlights the necessity of correct timing of FGF and BMP signaling.

Results

Thyroid specification is a multi-step event

In zebrafish, the thyroid specification is currently defined by the co-expression of *pax2a* and *nkx2.4b*. Therefore, thyroid progenitors have to express both of these markers to be considered as actual thyroid progenitors and in this context, *pax2a* and *nkx2.4b* are considered equal (Wendl et al., 2002). However, no report has characterized in detail the expression of these markers in the early thyroid progenitors *in vivo*. Thus, a comprehensive characterization of the main thyroid specification markers is crucial for accurate analysis of early thyroid development phenotypes. To do so, we analyzed the co-expression of *pax2a* and *nkx2.4b* by performing cell counting on entire thyroid primordia isolated from immunostained 18 to 55 hpf Et(*nkx2.4b*:YFP) (Ellingsen et al., 2005) zebrafish embryos.

Surprisingly, we could count an average of 12,1 (n=9) endodermal cells that express detectable levels of the Pax2a protein at 20 hpf (Fig. 1A), 4 hours before the event currently defined as the thyroid specification. Moreover, embryos as young as 18 hpf showed few but clearly detectable Pax2a-expressing endodermal cells (data not shown). The number of Pax2a-expressing cells in the foregut endoderm increases from 20 to 28 hpf, when it peaks at an average of 65,9 cells (n=26). Then, the number of Pax2a-expressing cells progressively decreases down to 31,7 (n=3) until 55 hpf. In contrast, no expression of YFP could be detected in Et(*nkx2.4b*:YFP) embryos before 22 hpf, indicating that *nkx2.4b* is not expressed. Still, only a

faint signal could be observed at this stage in 3,1 endoderm cells, on average (n=12) (Fig. 1A). The number of YFP-positive cells increases between 22 and 24 hpf and remains relatively stable until 55 hpf with a global average of 21,5 (n=48). We observed a similar time-lag between the expression of *pax2a* and *nkx2.4b* by whole mount *in situ* hybridization (WISH) (data not shown).

The ratio of Pax2a- and YFP- double positive cells increases between 24 and 55 hpf and this increase is solely due to the reduction in the Pax2a-expressing cell number. By 55 hpf, the majority of the thyroid progenitors co-expresses Pax2a and YFP (Fig. 1) and, although no cell counting has been performed at 80 hpf, it appeared under the confocal microscope that every thyroid progenitor co-expresses Pax2a and YFP (Fig. 1B). Interestingly, about half of the initial precursors will never activate *nkx2.4b* and these cells progressively disappear. Also, the YFP expression was always detected in the cells that already express Pax2a (Fig. 1B) and, the co-expression of the two appeared patterned (Fig. S1): The co-expression levels were higher in the anterior domain and in proximity with the heart tube. Yet, in agre(Wendl et al., 2002), the YFP expression was unchanged in CRISPR-Cas9-mediated *pax2a* knock-down Et(*nkx2.4b*:YFP) embryos, indicating that *nkx2.4b* is independent from *pax2a* (Fig. S2).

Taken together, these data highlights two major discrepancies with the current literature: First, Pax2a is expressed much earlier in the thyroid progenitors than we previously thought and second, the Pax2a-expressing endodermal cell population between 22 and 55 hpf is on average more than twice larger than the YFP-positive one. Therefore, this indicates that the thyroid specification occurs in at least two steps: The expression of Pax2a in a relatively large domain of the foregut endoderm from 18 hpf and, the expression of Nkx2.4b — as revealed by the Et(*nkx2.4b*) line — in a subset of the Pax2a-positive cells from 22/24 hpf. Thus, these two distinct steps define a new intermediate cell population which we term thyroid precursors. The precursors seem to be committed toward a thyroid fate but are not fully specified as they express Pax2a only. Only the fully specified thyroid progenitors will remain and eventually form the adult thyroid tissue.

FGF and BMP activities coincide with pax2a and nkx2.4b activation

Recently, we showed that the FGF and BMP morphogen signaling pathways are the two most important ones for early zebrafish thyroid development (Haerlingen et al., 2019). However, it remains unclear whether FGF and BMP signal directly the foregut endoderm or via an intermediate tissue. Thus, we used the validated Tg(*dusp6*:d2EGFP) (Molina et al., 2007) and Tg(BRE:dmKO2) (Collery and Link, 2011) zebrafish biosensor lines, which respectively report

the FGF or BMP activity, to map the activity of these pathways in the foregut endoderm during early thyroid development.

Such analysis revealed that the first detectable d2EGFP signals appear around 18/19 hpf in the Pax2a-positive thyroid precursors (Fig. S3). From this stage, the number of thyroid precursors with d2EGFP signal increases until 26/28 hpf (Fig. 2A, E), similar to the thyroid precursors number. As a result, about 80% of the thyroid precursors (n=48) displays a clear d2EGFP signal (Fig. 2B, E), suggesting a possible correlation between FGF and the *pax2a* activation. In contrast, very few, if any, thyroid precursors show dmKO2 signal before 22 hpf. From this point onwards, their number starts to increase and reaches proportions of thyroid precursors comparable to those with d2EGFP signal (Fig. 2C-E). On the other hand, most of the YFP-positive thyroid progenitors show clear dmKO2 signal during specification (Fig. S3). Thus, the temporal dynamics of dmKO2 appear to replicate that of YFP in Tg(BRE:dmKO2),Et(*nkx2.4b*:YFP) embryos. This could suggest a link between BMP and *nkx2.4b*, just like that, between FGF and *pax2a*. To be noted, the most intense d2GFP and dmKO2 signals were observed in the thyroid precursors near the heart tube (Fig. 2E), further supporting the cardiac origins of the FGF and BMP signals that we recently proposed (Vandernoot et al., 2019).

Correct timing of BMP and FGF is essential for thyroid specification

Although it is now clear that FGF and BMP are master regulators of early thyroid development, very limited data regarding the timing of these pathways are available. Wendl and colleagues performed short FGF inhibitions during the segmentation stage and observed that thyroid development was impaired by any of their short FGF inhibitions. Similarly, we sought here to dissect the dynamic functions of FGF and BMP in early thyroid development during segmentation stage by applying FGF or BMP inhibitors, PD166866 and DMH1 respectively, for 3-hours periods of time (10-13, 13-16, 16-19, 19-21 and, 21-24 hpf) covering the entire segmentation stage.

It appears from these short inhibitions that the BMP pathway might play two roles in early thyroid development. As expected from our previous report, BMP inhibition, using DMH1 during the entire segmentation stage, led to the absence of thyroid progenitors, as inferred from the loss of *nkx2.4b* and *tg* expression by WISH. Interestingly, the earliest short BMP inhibition (10-13 hpf) also caused a loss of thyroid markers at 28 and 55 hpf (Fig. 3 and S4). Mid-segmentation (13-16 and 16-19 hpf) DMH1 treatments caused only very mild reduction in the *nkx2.4b* expression at 28 hpf and *tg* expression appeared unaffected at 55 hpf. However, late segmentation (19-21 and 21-24 hpf) BMP inhibitions led to dramatic reduction in *nkx2.4b* and

particularly *tg* expression respectively at 28 and 55 hpf (Fig. 3 and S4A), highlighting a potential second BMP-sensitive period. The 10-13 hpf BMP inhibitions induced a similar reduction in the Pax2a expression, as observed by immunofluorescence, but the late segmentation inhibitions did not affect Pax2a expression. Unexpectedly, the short FGF inhibitions using PD166866 left the *nkx2.4b* and *tg* expression unaffected whereas whole segmentation stage-treatment blocked them (Fig. 3 and Haerlingen et al., 2019). Cell counting however indicated that Pax2a progressively reduced as the PD166866 was applied later during the segmentation stage (Fig. S4B).

Thus, in zebrafish, it appears that BMP could play biphasic role, at early and late segmentation stage. The first one could be a patterning effect whereas the second one could be the regulation of the thyroid specification itself, perhaps through *nkx2.4b* regulation, in agreement with the data presented above. FGF, on the other hand, appears to be required for a prolonged period of the segmentation stage and short inhibitions have very mild effects on thyroid specification. This discrepancy with the Wendl's findings remains unexplained.

FGF over-activation at late segmentation increases thyroid primordium size

Even though the short FGF inhibitions did not affect early thyroid development, we investigated more in detail the functions of FGF in thyroid specification because it is clear from the present report and previous studies including ours (Haerlingen et al., 2019; Kurmann et al., 2015; Wendl et al., 2007) that FGF is a crucial factor in thyroid specification. We over-activated FGF at 10, 15 and/or 20 hpf using the heat-shock-inducible Tg(*hsp70*:ca-fgfr1) zebrafish line (Marques et al., 2008) to have an early, mid, late, and whole segmentation stage over-activations that match with the previous short inhibitions. Shorter intervals were not considered due to the expected effect duration of a single heat-shock.

FGF over-activation at 10 hpf did not produce any noticeable difference in the *nkx2.4b* expression assessed by WISH between the heat-shocked Tg(*hsp70*:ca-fgfr1) and control embryos (Fig. 4A). On the contrary, FGF over-activation at 15 or 20 hpf led to obvious thyroid enlargement. WISH analyses of the *nkx2.4b* expression showed that approximatively 20 and 25% of the heat-shocked embryos had either a thyroid primordium that extends along the AP axis or an extra ectopic domain (Fig. 4A and B). It should be noted here that the Tg(*hsp70*:ca-fgfr1) founders are maintained as hemizygous and transgenic embryos could not be sorted out morphologically. Upon genotyping embryos heat-shocked at 20 hpf , we found a 100% correlation between the enlarged thyroid and the *hsp70*:ca-fgfr1 transgene. However, only a 50% correlation — which corresponds to a random distribution — was found in embryos heat-

shocked at 15 hpf (data not shown), an indication that one should consider the data from this condition carefully.

Cell counting showed that clusters of embryos heat-shocked at 15 or 20 hpf had a higher number of Pax2a-positive thyroid precursors at both 22 and 28 hpf compared to non-heat-shocked siblings (the absence of genotype sorting makes it appear non-significant). As for the number of YFP-positive thyroid progenitors in Et(*nkx2.4b*:YFP) embryos, it was higher at both stages when FGF was over-activated at 15 hpf but was higher only at 28 hpf when FGF was over-activated at 20 hpf (Fig. 4C). Thus, this indicates that the FGF pathway might promote thyroid specification by regulating the expression of *pax2a*, but not of *nkx2.4b*. In other words, it initiates the first step of thyroid specification: the emergence of the thyroid precursors. In this hypothesis, the increase in the YFP-positive progenitors' number would be an indirect consequence of the increased Pax2a-positive precursors number.

BMP over-activation causes premature and enhanced thyroid specification

In order to test the biphasic role of BMP identified above, we over-activated the BMP pathway using a similar approach as we did for FGF: we heat-shocked inducible Tg(*hsp70*:*bmp2b*) embryos (Chocron et al., 2007), at the same stages. *nkx2.4b* expression analysis by WISH at 28 hpf showed that BMP over-activation during early segmentation causes a striking thyroid enlargement compared to their WT or non-heat-shocked siblings (Fig. 5A,B and S5). After such a BMP over-activation, the thyroid primordium consists of a midline stripe that extends abnormally along the AP axis. Analysis of the *foxa2* expression shows that the entire foregut has major left-right asymmetry defects, possibly explaining the abnormal thyroid morphology. Analysis of the profiles of *foxa3* by WISH and *sox17* in Tg(*hsp70*:*bmp2b*,*sox17*:EGFP) embryos (Mizoguchi et al., 2008) indicated that the AP axis patterning was unaffected (Fig. S5 and data not shown). However, confocal imaging showed that the thyroid primordium is now a solid rod in which we could detect thyroid precursors along the entire DV axis (Fig. 5C), suggesting a disruption of that axis (De Felice and Di Lauro, 2004).

Further cell counting analysis revealed that at 22 hpf the number of Pax2a-positive precursors was unchanged in most of the Tg(*hsp70*:*bmp2b*) embryos heat-shocked at 10 hpf whereas the number of progenitors expressing YFP was on average 6,7 times larger than in their non-heat-shocked siblings (Fig. 5D). At 28 hpf, we observed a 3- and 5-fold increase in the number of Pax2a and YFP-positive thyroid progenitors, respectively. The increase in thyroid progenitor number seems to be permanent as number of cells expressing Pax2a or YFP in Tg(*hsp70*:*bmp2b*),Et(*nkx2.4b*:YFP) embryos were on average 3 times higher compared to control embryos at all investigated stages until 55 hpf (Fig. S5C and D). Concomitantly, the heart

was also severely abnormal: in Tg(*hsp70*:*bmp2b*) embryos, and it usually adopted a drop-like shape with one or two tails running caudally. Occasionally, the heart fields did not fuse at all. Despite their severe morphology defects, the heart and foregut endoderm maintained their close physical contacts (Fig. S5B and data not shown). 10-15-20 hpf serial BMP over-activations replicated these phenotypes.

We also found by cell counting that at 22 hpf, mid or late segmentation (15 or 20 hpf) over-activations caused an enlargement of the Pax2a-positive thyroid precursor population in about half of the heat-shocked embryos, accompanied by a premature YFP signal. Of note, like the Tg(*hsp70*:ca-fgfr1) line, the Tg(*hsp70*:*bmp2b*) founders are maintained in a heterozygous state, which means that half of the embryos are non-transgenic. Given that the 15 and 20 hpf heat-shocks did not induce gross morphology defects, these embryos were not sorted out, unlike the embryos heat-shocked at 10 hpf. However, genotyping of heat-shocked embryos showed an over 80% phenotype-genotype association (data not shown). At 28 hpf, we observed by WISH in about one-third of all embryos a noticeable increase in the *nkx2.4b* expression domain size. In this case, the thyroid primordium appeared larger on the AP axis. We observed a similar trend in the number of Pax2a and YFP-positive thyroid progenitors by confocal imaging (Fig. 5).

In brief, all BMP over-activations led to amplified or premature thyroid specification. The amplification was observed after BMP over-activation at 10 hpf whereas the premature specification was seen after heat-shock at 15 or 20 hpf. Thus, all of these data are in line with the previous statements: First, it confirms that BMP acts at two different times, during early and late segmentation stage, through distinct mechanisms. Second, it supports the hypothesis that BMP regulates the activation of *nkx2.4b*. Indeed, the premature and enlarged YFP expression in Et(*nkx2.4b*:YFP) embryos supports it too. Though, it does not explain the enlarged Pax2a-positive thyroid precursors population.

Early segmentation BMP acts upstream of FGF to regulate thyroid specification

Given the striking phenotype induced by the BMP over-activation at 10 hpf despite the very long recovery time between the heat-shock and the actual thyroid specification, we looked for possible mechanisms. Because the FGF pathway is a key regulator of the thyroid specification, we analyzed its activity after 4-hours long DMH1 treatment with the previously used Tg(*dusp6*:d2EGFP) zebrafish line. As a proof of principle, we performed PD166866 treatment following the same timing.

In normal conditions, most of the thyroid precursors have obvious d2EGFP staining and represents the majority of the endodermal d2EGFP-positive cells (see above) at 22 hpf. As

expected, we observed a gradual reduction in d2EGFP as we applied PD166866 for gradually shorter duration before sampling. PD166866 treatment between 10 and 14 hpf had no significant effect on the d2EGFP signal, probably because the embryos recovered normal FGF levels after drug washout. All other PD166866 treatments caused a robust reduction in the d2EGFP signal in thyroid precursors (Fig. 6A). Surprisingly, DMH1 treatments also led to severe d2EGFP signal reduction. The treatments covering early segmentation (10-14 and 10-22 hpf) caused a near-complete loss of d2EGFP in the thyroid progenitors (Fig. 6A). Later DMH1 treatments during the segmentation stage caused milder d2EGFP reduction. These observations indicate that the role in thyroid specification played by BMP during early segmentation stage involves a regulation of the foregut endoderm capacity to respond, later during thyroid specification, to FGF signals. Hence, the striking thyroid phenotypes resulting from early BMP over-activation or inhibition might be due to the enhanced or suppressed FGF responsiveness of the future thyroid precursors, respectively.

Interestingly, no such short PD166866 or DMH1 treatments caused a significant d2EGFP reduction in the non-thyroid precursor endodermal cells of 22 hpf Tg(*dusp6*:d2EGFP) embryos, whereas whole segmentation PD166866 treatment did (Fig. S6). Therefore, the different responses to the same treatment might suggest that there are already differences between the molecular signature of the future thyroid precursors and that of the other endodermal cells at the beginning of the segmentation stage, before 14 hpf. This could further suggest that the future thyroid precursors are already partially committed in some extend to a thyroid fate and might represent a third step of thyroid specification. This hypothesis still has to be tested.

Coordinated FGF and BMP governs early thyroid development

It has been previously shown in pancreas for example that FGF and BMP cooperate to regulate the transcription of endodermal and pancreatic genes (Guo and Wang, 2009; X. Xu et al., 2011) but no such data are available for the thyroid. Thus, to investigate the possible interactions between the FGF and BMP signaling pathways in early thyroid development, we crossed the Tg(*hsp70*:ca-fgfr1) and Tg(*hsp70*:*bmp2b*) heat-shock inducible lines to generate double transgenic embryos, which will allow us to simultaneously over-activate FGF and BMP following the same timings than above (10, 15 and/or 20 hpf) and assess the impacts on thyroid specification.

As expected, all single FGF or BMP over-activations recapitulated the results described above (see Fig. 4 and 5). Combined FGF and BMP over-activation at 10 hpf caused a highly similar phenotype to that of a single BMP over-activation, consistent with the observation that FGF over-activation at 10 hpf does not affect the thyroid significantly. However, in the

Tg(*hsp70*:ca-fgr1,*hsp70*:*bmp2b*) embryos, the serial 10-15-20 hpf heat-shocks did amplify the already dramatic phenotype induced by the single BMP over-activation at 10 hpf. In these embryos, the *nkx2.4b* expression domain assessed by WISH staining appeared even more extended on the AP axis than in Tg(*hsp70*:*bmp2b*) embryos heat-shocked at the same time (data not shown).

Similarly, the double FGF-BMP over-activations at 15 and 20 hpf amplified the thyroid enlargement obtained after single over-activation of either FGF or BMP, particularly the 20 hpf over-activation (Fig. 6B, C). Following the latter, some embryos displayed an extremely enlarged thyroid primordium, as depicted by *nkx2.4b* WISH staining. It consisted of an important caudal extension with robust *nkx2.4b* expression. Other than the extension, shape and location were normal. Genotyping confirmed the correlation between the extremely enlarged thyroid phenotype and the Tg(*hsp70*:ca-fgr1,*hsp70*:*bmp2b*) genotype in about 75% of the embryos. This relatively low correlation rate might be due to the subjective classification as *enlarged* or *extremely enlarged*. As we assume that the FGF or BMP pathways are saturated after their respective over-activation via heat-shock, these data indicate that FGF and BMP regulate distinct aspects of thyroid specification, possibly the activation of *pax2a* and *nkx2.4b*.

Next, we wanted to know whether these independent regulations are both fully required or whether one can compensate for the loss of the other. To study this, we modulated the FGF and BMP pathways simultaneously but in the opposite ways: if we over-activate FGF, we inhibit BMP and *vice versa* and looked for possible rescue of *pax2a* or *nkx2.4b* expression. For the over-activations, we again used the heat-shock-inducible Tg(*hsp70*:ca-fgfr1) and Tg(*hsp70*:*bmp2b*) lines and applied the heat-shock at 10, 15 and/or 20 hpf. Chemical inhibitors, PD166866 and DMH1, were applied continuously between 10 and 26 hpf.

Interestingly, most of the FGF and BMP over-activation times failed to rescue the *nkx2.4b* expression in DMH1- or PD166866-treated embryos, as depicted by the loss of *nkx2.4b* WISH staining in the foregut endoderm (Fig. 6D). The only exception was the serial heat-shocks of 10-15-20 hpf of Tg(*hsp70*:*bmp2b*) embryos. In these embryos, a disorganized *nkx2.4b* expression domain was detected in the foregut despite the PD166866-mediated FGF inhibition. This shows that a sustained BMP over-activation can compensate for the loss of FGF activity and rescue the thyroidal *nkx2.4b* expression, at least partially. Preliminary observations indicate that, despite rescue of *nkx2.4b* expression, serial BMP over-activation did not rescue Pax2a expression. However, it seems that FGF over-activation during late segmentation — single 20 hpf and serial heat-shock at 10-15-20 hpf— could partially restore the Pax2a-positive

progenitors' number (data not shown). Altogether, these data show that both the FGF and BMP pathways are crucial for complete thyroid specification. Yet, specific over-activation of FGF in BMP-inhibited embryos and of BMP in FGF-inhibited embryos can rescue part of the expression of *pax2a* or *nkx2.4b*, respectively. Thus, these data further support the hypothesis that FGF and BMP regulates respectively *pax2a* and *nkx2.4b*.

Discussion

The data presented in this study provide novel insights into thyroid specification and most importantly, the underlying molecular mechanisms that occur before. We also identified how extrinsic factors regulate this process and proposed an updated definition of the thyroid specification. Specifically, we found major differences between the expression profiles of *pax2a* and *nkx2.4b*. *pax2a* is detectable in the foregut endoderm from 18 hpf and the number of Pax2a-positive cells in the foregut rapidly increases until 28 hpf. In contrast, no *nkx2.4b* expression can be detected before 22/24 hpf and from that stage, only a subpopulation of the Pax2a-positive cells activates the *nkx2.4b* expression.

The interval between the onset of the two genes and the larger cell population marked by Pax2a define the two steps and the two types of thyroid progenitors of our updated thyroid specification definition: The first step consists in the emergence of the thyroid precursors from 18 hpf. The thyroid precursors are a newly identified transient cell population that expresses *pax2a,* but not *nkx2.4b,* and represents a semi-specified state; they are *committed* toward thyroid fate but not fully specified yet. The second step is the appearance of the thyroid progenitors within the thyroid precursors from 22/24 hpf. The thyroid progenitors differ from the precursors in that they express *nkx2.4b* and therefore, are now fully specified for thyroid fate and will eventually form the mature thyroid tissue. Noteworthy, only half of the thyroid precursors will turn into progenitors and those that will not activate *nkx2.4b* will disappear. It is currently unclear whether the "surplus" of thyroid precursors plays any roles or whether it is only a side product of an excessively efficient thyroid precursor differentiation. Still, given that hypoplasic thyroids cannot catch up a normal size (Lania et al., 2009; Trubiroha et al., 2018) — perhaps due to limited proliferation capacity — we postulate that it is a way to ensure sufficient adult thyroid's size, like what happens in pancreas (Stanger et al., 2007). Similar sequential activation of the main markers has also been proposed for other endoderm-derived organs (Wandzioch and Zaret, 2009).

Our data also indicate that FGF and BMP act in a precise sequence throughout the segmentation period to initiate thyroid specification. First, we found that BMP plays a major role very early during the segmentation stage. Brief BMP modulations at this stage have surprisingly

dramatic effects on the thyroid specification, which occurs 10/12 hours later. The early segmentation BMP inhibitions also caused severe reductions in the FGF activity in the thyroid precursors and FGF is a major regulator of thyroid specification (Haerlingen et al., 2019; Kurmann et al., 2015; Wendl et al., 2007). Thus, we propose that BMP positively regulates the capacity of the foregut endoderm to respond to the thyroid fate-inducing FGF signals that emerge from 18 hpf. Because BMP regulates the dorsoventral (DV) axis through Sox2, which represses *Nkx2.1* in mouse and *Xenopus* lungs (Domyan et al., 2011; Trisno et al., 2018), another hypothesis is that a similar BMP-Sox2 cascade controls the *nkx2.4b* expression in the thyroid as well. Yet, it is also possible that the regulation of the FGF responsiveness and the induction of ventral fates by BMP are actually part of the same phenomenon: ventral fates could respond more to FGF signals. Either way, the molecular mechanism remains to be determined. Interestingly, the future thyroid precursors and the other endodermal cells do not respond the same way to the same early segmentation BMP modulation. These different responses indicate that the cells in the nascent foregut endoderm have different capacities to respond to BMP signals, which implies that they have different molecular signatures, and thus, might suggest a possible third step in thyroid specification.

Second, we found that during the actual thyroid specification, FGF acts on the endoderm a few hours before BMP. Our mapping data indicates that some endodermal cells display an apparent FGF activity from 18 hpf, which coincides with the activation of *pax2a* in the very same cells, the thyroid precursors. Importantly, the vast majority of the thyroid precursors are FGF-active and *vice versa*, which might suggest a transcriptional regulation of *pax2a* by the FGF pathway. Although we have not tested this hypothesis experimentally, reports have demonstrated this direct regulation in the otic vesicle (Hans et al., 2004; McCarroll et al., 2012). Moreover, the observations that (1) short late segmentation FGF inhibitions reduces the number of Pax2a-positive cells but leaves unaffected *nkx2.4b* and (2) that FGF over-activation does increase the number of Pax2a-positive thyroid precursors but not that of *nkx2.4b*-positive thyroid progenitors at 22 hpf support this hypothesis. Still, it remains unclear why the number of *nkx2.4b*-positive thyroid progenitors was higher in these embryos at 28 hpf and in embryos heat-shocked at 15 hpf. Given the interval between the heat-shock and sampling, it is possible that this observed increase is an indirect consequence of the enlarged initial pool *pax2a*-positive thyroid precursors.

We also showed that the BMP activity in the thyroid precursors rises concurrently with the activation of *nkx2.4b* in the thyroid progenitors and just like FGF is active in most of the thyroid

precursors, BMP seems to be active in most of the *nkx2.4b*-expressing thyroid progenitors. The short BMP inhibitions at the time of thyroid specification repress the *nkx2.4b* expression while it leaves unaffected the Pax2a expression. In contrast, the corresponding over-activations tend to increase the expression of both *pax2a* and *nkx2.4b* at 22 and 28 hpf. This dual phenotype poorly fits with a sole direct transcriptional regulation but rather supports the presence of an additional intermediate regulator. In lungs, it has been shown that such an indirect regulation involves the repression of Sox2, which is a dorsal fate marker that represses lung markers like *Nkx2.1* (Domyan et al., 2011; Trisno et al., 2018). Thus, we consider that it is very likely that such an indirect regulation, perhaps involving Sox2, also occurs during early thyroid development. Considering that (1) BMP4 is the effective BMP ligand in lungs, (2) BMP4 is strongly expressed in the cardiac mesoderm at the time of thyroid specification and (3) BMP4 is used in *in vitro* thyroid differentiation (Chen et al., 1997; Longmire et al., 2012; Trisno et al., 2018), we hypothesise that BMP4 could be the thyroid fate-inducing BMP ligand and that its over-expression, instead of *bmp2b*, would activate *nkx2.4b* expression far more efficiently.

The hypothesis that FGF and BMP respectively regulate *pax2a* and *nkx2.4b* is consistent with the massive enlargement observed after double FGF and BMP over-activation at 20 hpf. According to this hypothesis, FGF enlarges the Pax2a-positive thyroid precursors population, in which an increased proportion would activate *nkx2.4b* upon BMP signaling. Moreover, the partial rescue of *pax2a* expression after FGF over-activation in BMP-inhibited embryos and, of *nkx2.4b* after robust BMP over-activation in FGF-inhibited embryos further support this hypothesis.

Altogether, these data bring novel insights into early thyroid development and, combined with our previous studies (Vandernoot et al., 2019), led us to propose an updated model of thyroid specification (Fig. 7). In our model, around 10/13 hpf, the newly formed foregut endoderm receives BMP signals from the aLPM hpf. These signals will make it FGF-sensitive. This FGF sensitization might be part of the establishment of the DV axis. From 18 hpf, the cardiac mesoderm continuously provides FGF signaling to the anterior foregut endoderm. As a result, a large endodermal population would activate *pax2a* to generate the thyroid precursors, a semi-differentiated state. From 22/24 hpf, the cardiac mesoderm provides a second wave of BMP signals — likely BMP4 — that activates the *nkx2.4b* expression, through a direct transcriptional regulation and possibly an intermediate regulator, in a subset of the thyroid precursors, hence forming the thyroid progenitors. The thyroid precursors that do not turn into thyroid progenitors will eventually disappear; only the true thyroid progenitors will functionally differentiate and form the mature thyroid tissue. The observation that *nkx2.4b* is activated only in cells that already express *pax2a* but does not rely on it implies a common origin or nearby sources of the FGF and

BMP ligands, the cardiac mesoderm in our model. This model is in line with the FGF permissive functions proposed by Wendl and colleagues (Wendl et al., 2007) and we postulate here that BMP is the missing inductive factor. This model highlights that few signalling pathways are required for thyroid development but, like in early lung development, their «*timing is everything*» (Rankin et al., 2018).

Acknowledgments

The authors would like to thank Jean-Marie Vanderwinden and staff from the Light Microscopy Facility for confocal microscopy assistance.

Author Contributions

B.H. performed the experiments and wrote the manuscript; R.O. supervised most of the experiments. A.M. and I.V. helped to perform the BMP and FGF activity inhibition and mapping experiments. P.G. and M.S. helped with the Sox2 experiments. B.H., R.O., and S.C. designed the experiments and interpreted the data with the help of A.T.. M.S. and S.C. edited the manuscript.

Declaration of Interests

The authors declare no conflicts of interest.

References

Alt, B., Reibe, S., Feitosa, N.M., Elsalini, O.A., Wendl, T., Rohr, K.B., 2006. Analysis of origin and growth of the thyroid gland in zebrafish. Dev. Dyn. 235, 1872–1883. doi:10.1002/dvdy.20831

Bernal, J., 2007. Thyroid hormone receptors in brain development and function. Nature Clinical Practice Endocrinology & Metabolism 3, 249 EP – –259. doi:10.1038/ncpendmet0424

Buchholz, D.R., Paul, B.D., Fu, L., Shi, Y.-B., 2006. Molecular and developmental analyses of thyroid hormone receptor function in Xenopus laevis, the African clawed frog. General and Comparative Endocrinology 145, 1–19. doi:10.1016/j.ygcen.2005.07.009

Celli, G., LaRochelle, W.J., Mackem, S., Sharp, R., Merlino, G., 1998. Soluble dominant-negative receptor uncovers essential roles for fibroblast growth factors in multi-organ induction and patterning. EMBO J 17, 1642–1655. doi:10.1093/emboj/17.6.1642

Chen, J.N., van Eeden, F.J., Warren, K.S., Chin, A., Nüsslein-Volhard, C., Haffter, P., Fishman, M.C., 1997. Left-right pattern of cardiac BMP4 may drive asymmetry of the heart in zebrafish. Development 124, 4373–4382. doi:10.1038/383407a0

Chocron, S., Verhoeven, M.C., Rentzsch, F., Hammerschmidt, M., Bakkers, J., 2007. Zebrafish Bmp4 regulates left-right asymmetry at two distinct developmental time points. Developmental Biology 305, 577–588. doi:10.1016/j.ydbio.2007.03.001

Collery, R.F., Link, B.A., 2011. Dynamic smad-mediated BMP signaling revealed through transgenic zebrafish. Dev. Dyn. 240, 712–722. doi:10.1002/dvdy.22567

Corbetta, C., Weber, G., Cortinovis, F., Calebiro, D., Passoni, A., Vigone, M.C., Beck-Peccoz, P., Chiumello, G., Persani, L., 2009. A 7-year experience with low blood TSH cutoff levels for neonatal screening reveals an unsuspected frequency of congenital hypothyroidism (CH). Clin. Endocrinol. (Oxf) 71, 739–745. doi:10.1111/j.1365-2265.2009.03568.x

De Felice, M., Di Lauro, R., 2004. Thyroid Development and Its Disorders: Genetics and Molecular Mechanisms. Endocrine Reviews 25, 722–746. doi:10.1210/er.2003-0028

Domyan, E.T., Ferretti, E., Throckmorton, K., Mishina, Y., Nicolis, S.K., Sun, X., 2011. Signaling through BMP receptors promotes respiratory identity in the foregut via repression of Sox2. Development 138, 971–981. doi:10.1242/dev.053694

Ellingsen, S., Laplante, M.A., König, M., Kikuta, H., Furmanek, T., Hoivik, E.A., Becker, T.S., 2005. Large-scale enhancer detection in the zebrafish genome. Development 132, 3799–3811. doi:10.1242/dev.01951

Fagman, H., Andersson, L., Nilsson, M., 2006. The developing mouse thyroid: embryonic vessel contacts and parenchymal growth pattern during specification, budding, migration, and lobulation. Dev. Dyn. 235, 444–455. doi:10.1002/dvdy.20653

Fagman, H., Nilsson, M., 2011. Morphogenetics of early thyroid development. J Mol Endocrinol 46, R33–42.

Gordillo, M., Evans, T., Gouon-Evans, V., 2015. Orchestrating liver development. Development 142, 2094–2108. doi:10.1242/dev.114215

Guo, X., Wang, X.-F., 2009. Signaling cross-talk between TGF-β/BMP and other pathways. Cell Res. 19, 71–88. doi:10.1038/cr.2008.302

Haerlingen, B., Opitz, R., Vandernoot, I., Trubiroha, A., Gillotay, P., Giusti, N., Costagliola, S., 2019. Small-Molecule Screening in Zebrafish Embryos Identifies Signaling Pathways Regulating Early Thyroid Development. Thyroid 29, 1683–1703. doi:10.1089/thy.2019.0122

Hans, S., Liu, D., Westerfield, M., 2004. Pax8 and Pax2a function synergistically in otic specification, downstream of the Foxi1 and Dlx3b transcription factors. Development 131, 5091–5102. doi:10.1242/dev.01346

Herriges, M., Morrisey, E.E., 2014. Lung development: orchestrating the generation and regeneration of a complex organ. Development 141, 502–513. doi:10.1242/dev.098186

Huang, C.-J., Tu, C.-T., Hsiao, C.-D., Hsieh, F.-J., Tsai, H.-J., 2003. Germ-line transmission of a myocardium-specific GFP transgene reveals critical regulatory elements in the cardiac myosin light chain 2 promoter of zebrafish. Dev. Dyn. 228, 30–40. doi:10.1002/dvdy.10356

Kimmel, C.B., Ballard, W.W., Kimmel, S.R., Ullmann, B., Schilling, T.F., 1995. Stages of embryonic development of the zebrafish. Dev. Dyn. 203, 253–310. doi:10.1002/aja.1002030302

Kimura, S., 1996. Thyroid-specific enhancer-binding protein: Role in thyroid function and organogenesis. Trends in Endocrinology & Metabolism 7, 247–252. doi:10.1016/S1043-2760(96)00115-4

Kimura, S., Hara, Y., Pineau, T., Fernandez-Salguero, P., Fox, C.H., Ward, J.M., Gonzalez, F.J., 1996. The T/ebp null mouse: thyroid-specific enhancer-binding protein is essential for the organogenesis of the thyroid, lung, ventral forebrain, and pituitary. Genes & Development 10, 60–69. doi:10.1101/gad.10.1.60

Kurmann, A.A., Serra, M., Hawkins, F., Rankin, S.A., Mori, M., Astapova, I., Ullas, S., Lin, S., Bilodeau, M., Rossant, J., Jean, J.C., Ikonomou, L., Deterding, R.R., Shannon, J.M., Zorn, A.M., Hollenberg, A.N., Kotton, D.N., 2015. Regeneration of Thyroid Function by Transplantation of Differentiated Pluripotent Stem Cells. Cell Stem Cell 17, 527–542. doi:10.1016/j.stem.2015.09.004

Lania, G., Zhang, Z., Huynh, T., Caprio, C., Moon, A.M., Vitelli, F., Baldini, A., 2009. Early thyroid development requires a Tbx1–Fgf8 pathway. Developmental Biology 328, 109–117. doi:10.1016/j.ydbio.2009.01.014

Longmire, T.A., Ikonomou, L., Hawkins, F., Christodoulou, C., Cao, Y., Jean, J.C., Kwok, L.W., Mou, H., Rajagopal, J., Shen, S.S., Dowton, A.A., Serra, M., Weiss, D.J., Green, M.D., Snoeck, H.-W., Ramirez, M.I., Kotton, D.N., 2012. Efficient derivation of purified lung and thyroid progenitors from embryonic stem cells. Cell Stem Cell 10, 398–411. doi:10.1016/j.stem.2012.01.019

Mansouri, A., Chowdhury, K., Gruss, P., 1998. Follicular cells of the thyroid gland require Pax8 gene function. Nat. Genet. 19, 87–90. doi:10.1038/ng0598-87

Marques, S.R., Lee, Y., Poss, K.D., Yelon, D., 2008. Reiterative roles for FGF signaling in the establishment of size and proportion of the zebrafish heart. Developmental Biology 321, 397–406. doi:10.1016/j.ydbio.2008.06.033

McCarroll, M.N., Lewis, Z.R., Culbertson, M.D., Martin, B.L., Kimelman, D., Nechiporuk, A.V., 2012. Graded levels of Pax2a and Pax8 regulate cell differentiation during sensory placode formation. Development 139, 2740–2750. doi:10.1242/dev.076075

Mizoguchi, T., Verkade, H., Heath, J.K., Kuroiwa, A., Kikuchi, Y., 2008. Sdf1/Cxcr4 signaling controls the dorsal migration of endodermal cells during zebrafish gastrulation. Development 135, 2521–2529. doi:10.1242/dev.020107

Molina, G.A., Watkins, S.C., Tsang, M., 2007. Generation of FGF reporter transgenic zebrafish and their utility in chemical screens. BMC Dev Biol 7, 62. doi:10.1186/1471-213X-7-62

Mullur, R., Liu, Y.-Y., Brent, G.A., 2014. Thyroid Hormone Regulation of Metabolism. Physiol. Rev. 94, 355–382. doi:10.1152/physrev.00030.2013

Ohuchi, H., Hori, Y., Yamasaki, M., Harada, H., Sekine, K., Kato, S., Itoh, N., 2000. FGF10 acts as a major ligand for FGF receptor 2 IIIb in mouse multi-organ development. Biochemical and Biophysical Research Communications 277, 643–649. doi:10.1006/bbrc.2000.3721

Olivieri, A., Stazi, M.A., Mastroiacovo, P., Fazzini, C., Medda, E., Spagnolo, A., De Angelis, S., Grandolfo, M.E., Taruscio, D., Cordeddu, V., Sorcini, M., Study Group for Congenital Hypothyroidism, 2002. A population-based study on the frequency of additional congenital malformations in infants with congenital

hypothyroidism: data from the Italian Registry for Congenital Hypothyroidism (1991-1998). Journal of Clinical Endocrinology & Metabolism 87, 557–562. doi:10.1210/jcem.87.2.8235

Opitz, R., Maquet, E., Huisken, J., Antonica, F., Trubiroha, A., Pottier, G.L., Janssens, V.R., Costagliola, S., 2012. Transgenic zebrafish illuminate the dynamics of thyroid morphogenesis and its relationship to cardiovascular development. Developmental Biology 372, 203–216. doi:http://dx.doi.org/10.1016/j.ydbio.2012.09.011

Opitz, R., Maquet, E., Zoenen, M., Dadhich, R., Costagliola, S., 2011. TSH receptor function is required for normal thyroid differentiation in zebrafish. Mol. Endocrinol. 25, 1579–1599. doi:10.1210/me.2011-0046

Rankin, S.A., Han, L., McCracken, K.W., Kenny, A.P., Anglin, C.T., Grigg, E.A., Crawford, C.M., Wells, J.M., Shannon, J.M., Zorn, A.M., 2016. A Retinoic Acid-Hedgehog Cascade Coordinates Mesoderm-Inducing Signals and Endoderm Competence during Lung Specification. Cell Rep 16, 66–78. doi:10.1016/j.celrep.2016.05.060

Rankin, S.A., McCracken, K.W., Luedeke, D.M., Han, L., Wells, J.M., Shannon, J.M., Zorn, A.M., 2018. Timing is everything: Reiterative Wnt, BMP and RA signaling regulate developmental competence during endoderm organogenesis. Developmental Biology 434, 121–132. doi:10.1016/j.ydbio.2017.11.018

Revest, J.M., Spencer-Dene, B., Kerr, K., De Moerlooze, L., Rosewell, I., Dickson, C., 2001. Fibroblast growth factor receptor 2-IIIb acts upstream of Shh and Fgf4 and is required for limb bud maintenance but not for the induction of Fgf8, Fgf10, Msx1, or Bmp4. Developmental Biology 231, 47–62. doi:10.1006/dbio.2000.0144

Rohr, K.B., Concha, M.L., 2000. Expression of nk2.1a during early development of the thyroid gland in zebrafish. Mech Dev 95, 267–270. doi:http://dx.doi.org/10.1016/S0925-4773(00)00345-2

Serls, A.E., Doherty, S., Parvatiyar, P., Wells, J.M., Deutsch, G.H., 2005. Different thresholds of fibroblast growth factors pattern the ventral foregut into liver and lung. Development 132, 35–47. doi:10.1242/dev.01570

Spagnoli, F.M., 2007. From endoderm to pancreas: a multistep journey. Cell. Mol. Life Sci. 64, 2378–2390. doi:10.1007/s00018-007-7184-x

Stanger, B.Z., Tanaka, A.J., Melton, D.A., 2007. Organ size is limited by the number of embryonic progenitor cells in the pancreas but not the liver. Nature 445, 886–891. doi:10.1038/nature05537

Thisse, C., Thisse, B., 2008. High-resolution in situ hybridization to whole-mount zebrafish embryos. Nat Protoc 3, 59–69. doi:10.1038/nprot.2007.514

Thomas, P.Q., Brown, A., Beddington, R.S., 1998. Hex: a homeobox gene revealing peri-implantation asymmetry in the mouse embryo and an early transient marker of endothelial cell precursors. Development 125, 85–94.

Trisno, S.L., Philo, K.E.D., McCracken, K.W., Catá, E.M., Ruiz-Torres, S., Rankin, S.A., Han, L., Nasr, T., Chaturvedi, P., Rothenberg, M.E., Mandegar, M.A., Wells, S.I., Zorn, A.M., Wells, J.M., 2018. Esophageal Organoids from Human Pluripotent Stem Cells Delineate Sox2 Functions during Esophageal Specification. Cell Stem Cell 23, 501–515.e7. doi:10.1016/j.stem.2018.08.008

Trubiroha, A., Gillotay, P., Giusti, N., Gacquer, D., Libert, F., Lefort, A., Haerlingen, B., De Deken, X., Opitz, R., Costagliola, S., 2018. A Rapid CRISPR/Cas-based Mutagenesis Assay in Zebrafish for Identification of Genes Involved in Thyroid Morphogenesis and Function. Scientific Reports 8, 5647. doi:10.1038/s41598-018-24036-4

Vandernoot, I., Haerlingen, B., Trubiroha, A., Gillotay, P., Janssens, V., Opitz, R., Costagliola, S., 2019. Enhanced canonical Wnt signaling during early zebrafish development perturbs the interaction of cardiac mesoderm and pharyngeal endoderm and causes thyroid specification defects. bioRxiv 8, 2019.12.19.880815. doi:10.1101/2019.12.19.880815

Wandzioch, E., Zaret, K.S., 2009. Dynamic Signaling Network for the Specification of Embryonic Pancreas and Liver Progenitors. Science 324, 1707–1710. doi:10.1126/science.1174497

Wassner, A.J., 2018. Congenital Hypothyroidism. Endocrinology 45, 1–18. doi:10.1016/j.clp.2017.10.004

Wendl, T., Adzic, D., Schoenebeck, J., Scholpp, S., Brand, M., Yelon, D., Rohr, K., 2007. Early developmental specification of the thyroid gland depends on han-expressing surrounding tissue and on FGF signals. Development 134, 2871–2879. doi:10.1242/dev.02872

Wendl, T., Lun, K., Mione, M., Favor, J., Brand, M., Wilson, S.W., Rohr, K.B., 2002. Pax2.1 is required for the development of thyroid follicles in zebrafish. Development 129, 3751–3760.

Xu, H., Xiao, T., Chen, C.-H., Li, W., Meyer, C., Wu, Q., Wu, D., Cong, L., Zhang, F., Liu, J.S., Brown, M., Liu, S.X., 2015. Sequence determinants of improved CRISPR sgRNA design. Genome Research 25, 1147–1157. doi:10.1101/gr.191452.115

Xu, X., Browning, V.L., Odorico, J.S., 2011. Activin, BMP and FGF pathways cooperate to promote endoderm and pancreatic lineage cell differentiation from human embryonic stem cells. Mechanisms of Development 128, 412–427. doi:10.1016/j.mod.2011.08.001

Yelon, D., Horne, S.A., Stainier, D.Y.R., 1999. Restricted expression of cardiac myosin genes reveals regulated aspects of heart tube assembly

in zebrafish. Developmental Biology 214, 23–37. doi:10.1006/dbio.1999.9406

Zannini, M., Avantaggiato, V., Biffali, E., Arnone, M.I., Sato, K., Pischetola, M., Taylor, B.A., Phillips, S.J., Simeone, A., Di Lauro, R., 1997. TTF-2, a new forkhead protein, shows a temporal expression in the developing thyroid which is consistent with a role in controlling the onset of differentiation. The EMBO Journal 16, 3185–3197. doi:10.1093/emboj/16.11.3185

Figure Legends

Fig. 1: *pax2a* and *nkx2.4b* define two distinct cell populations in thyroid specification

(A) Evolution of number of endodermal cells expressing Pax2a (left pane), YFP (middle pane) and the ratio of YFP-positive cells co-expressing Pax2a (right pane) in Et(*nkx2.4b*:YFP) embryos. Bar: mean.

(B) Confocal images of thyroid primordia from Et(*nkx2.4b*:YFP) embryos co-immunostained with Pax2a and YFP antibodies at different stages. Yellow arrows: double Pax2a-YFP positive cells. Sagittal (26 to 55 hpf) and frontal sections (80 hpf). Scale bar: 25 μm.

Fig. 2: The FGF and BMP pathways are active during early thyroid development.

(A-B) Evolution of the absolute number of Pax2a-positive thyroid precursors with d2EGFP (A) or dmKO2 (B) signal (left panes) and of the proportions of the these thyroid precursors with the d2EGFP or dmKO2 signal (right panes) in Tg(*dusp6*:d2EGFP) or Tg(BRE:dmKO2) embryos, respectively. Bar: mean.

(C) Confocal image of thyroid primordia at different stages from Tg(*dusp6*:d2EGFP,BREdmKO2) embryos co-immunostained with Pax2a, GFP and dmKO2 antibodies. H: heart. Scale bar: 25 μm. See also Fig. S3.

Fig. 3: Short FGF or BMP inhibitions differentially affect thyroid specification

Relative frequencies of recovered thyroid phenotypes assessed by the expression of *nkx2.4b* at 28 hpf or *tg* at 55 hpf observed by WISH staining after small molecule-mediated inhibitions of FGF (PD166866) or BMP (DMH1). Targeted pathways and number of analyzed embryos are indicated above each bar. Compounds, concentrations and treatment periods (in brackets, in hpf) are indicated below each bar. Dotted pattern: abnormal morphology and/or location. See also Fig. S4.

Fig. 4: FGF over-activation enlarges the thyroid precursor population

(A) Relative frequencies of recovered thyroid phenotypes assessed by the expression of *nkx2.4b* at 28 hpf by WISH staining after heat-shock-induced FGF over-activation in Tg(*hsp70*:ca-fgfr1) at different times (indicated below each column). Number of analyzed embryos are indicated above each bar. Dotted pattern: abnormal morphology and/or location.

(B) Thyroid phenotypes induced by FGF over-activation at different times (indicated above each embryo) stained by WISH for *nkx2.4b* (blue) and *myl7* (red, cardiomyocytes). Hy: Hypothalamus. Scale bar: 200 μm.

(C) Absolute number of thyroid progenitors expressing Pax2a (1st and 3rd panes) and YFP (2nd and 4th panes) in 22 and 28 hpf Tg(*hsp70*:ca-fgfr1),Et(*nkx2.4b*:YFP) embryos after heat-shock-induced FGF over-activation at different times (indicated below each column). Note that

transgenic and non-transgenic Tg(*hsp70*:ca-fgfr1) embryos are plotted together. Statistical significance is indicated above each bar (see STAR methods for calculation method). Bar: mean.

Fig. 5: FGF over-activation leads to enlarged and premature thyroid

(A) Relative frequencies of recovered thyroid phenotypes assessed by the expression of *nkx2.4b* at 28 hpf by WISH staining after heat-shock-induced BMP over-activation in Tg(*hsp70*:*bmp2b*) at different times (indicated below each column). Number of analyzed embryos are indicated above each bar. Dotted pattern: abnormal morphology and/or location.

(B) Thyroid (upper lane) or foregut endoderm (lower lane) after BMP over-activation at different times (indicated above) stained by WISH for *nkx2.4b* and *myl7* (upper lane) or *foxa2* (lower lane). Hy: Hypothalamus. Scale bar: 200 μm.

(C) Confocal images of 28 hpf Tg(*hsp70*:*bmp2b*),Et(*nkx2.4b*:YFP) embryo thyroid after heat-shock-induced BMP over-activation at different times (indicated below each column) and co-immunostained with Pax2a, YFP and E-Cad antibodies. Scale bar: 25 μm.

(D) Absolute number of thyroid progenitors expressing Pax2a (1st and 3rd panes) and YFP (2nd and 4th panes) in 22 and 28 hpf Tg(*hsp70*:*bmp2b*),Et(*nkx2.4b*:YFP) embryos after heat-shock-induced BMP over-activation at different times (indicated below each column). Note that transgenic and non-transgenic Tg(*hsp70*:*bmp2b*) embryos heat-shocked at 15 and 20 hpf are plotted together. Statistical significance is indicated above each bar (see STAR methods for statistical method). Bar: mean.

Fig. 6: FGF and BMP cooperate to induce the thyroid fate

(A) Absolute number of thyroid precursors with d2EGFP signal in 22 hpf Tg(*dusp6*:d2EGFP) embryos treated with the FGF inhibitor PD166866 (left pane) or the BMP inhibitor DMH1 (right pane) during different short periods. Targeted pathway is indicated above each graph. Compounds, concentrations and treatment periods (in brackets, in hpf) are indicated below each column. Statistical significance is indicated above each column (see STAR methods for calculation method). Bar: mean.

(B) Relative frequencies of recovered thyroid phenotypes assessed by the expression of *nkx2.4b* at 28 hpf by WISH staining after heat-shock-induced double FGF and BMP over-activation in Tg(*hsp70*:ca-fgfr1,*hsp70*:*bmp2b*) at different times (indicated below each column). Number of analyzed embryos are indicated above each bar. Dotted pattern: abnormal morphology and/or location.

(C) Representative 28 hpf embryos from the four possible genotypes resulting from the breeding of Tg(*hsp70*:ca-fgfr1) and Tg(*hsp70*:*bmp2b*) founders (indicated above each embryo) stained by WISH for *nkx2.4b* and *myl7*. Scale bar: 200 μm.

(D) 28 hpf embryo thyroids after small molecule-mediated inhibition of FGF or BMP and/or heat-shocked mediated over-activation of BMP or FGF in Tg(*hsp70*:*bmp2b*) (upper lane) or Tg(*hsp70*:ca-fgfr1) (lower lane), respectively, and stained by WISH for *nkx2.4b* and *myl7*. All treatments are indicated above each embryo. Scale bar: 200 μm.

Fig. 7: Proposed updated model of the multi-step thyroid specification

See main text for details.

STAR Methods

LEAD CONTACT AND MATERIALS AVAILABILITY

Further information and requests for resources and reagents should be directed to and will be fulfilled by the Lead Contact, Sabine Costagliola (scostag@ulb.ac.be). This study did not generate new unique reagents, plasmids or animal lines.

EXPERIMENTAL MODEL AND SUBJECT DETAILS

Zebrafish husbandry and experiments with all transgenic lines will be performed under standard conditions as per the Federation of European Laboratory Animal Science Associations (FELASA) guideline, and in accordance with institutional (Université Libre de Bruxelles (ULB)) and national ethical and animal welfare guidelines and regulation, which were approved by the ethical committee for animal welfare (CEBEA) from the Université Libre de Bruxelles (protocols 578N-579N).

All embryos were collected within the next 15-20 minutes after they have been laid and kept at 28,5°C to ensure homogenous development. Embryos were staged as described by Kimmel and colleagues (Kimmel et al., 1995). Embryos were enzymatically dechorionated by incubation in embryo medium containing 0.6 mg/mL pronase at room temperature for 20-30 minutes before 24 hpf or sampling. Prior sampling, embryos were anesthetized with 0,02% tricaine and then fixed overnight in a 4°C 4% paraformaldehyde (PFA) solution in phosphate-buffered saline (PBS) on gentle agitation. The following zebrafish lines were used: Et(*nkx2.4b*:YFP) (CLGY576) (Ellingsen et al., 2005), Tg(*hsp70*:ca-fgfr1,*cryaa*:mCherry)^{pd1} (abbreviated as Tg(*hsp70*:ca-fgfr1)) (Marques et al., 2008), Tg(*hsp70*:*bmp2b*)^{fr13} (Chocron et al., 2007), Tg(-5.0*sox17*:EGFP)^{ha01} (abbreviated as Tg(*sox17*:EGFP)) (Mizoguchi et al., 2008), Tg(*myl7*:EGFP)^{twu26} (Huang et al., 2003), Tg(*dusp6*:d2EGFP)^{pt6} (Molina et al., 2007), Tg(BRE-AAVmlp:dmKO2)^{mw40} (abbreviated as Tg(BRE:dmKO2)) (Collery and Link, 2011).

METHOD DETAILS

Small molecule treatments

Stock solutions of PD166866 and DMH1 were prepared in DMSO at the concentration of 20 and 10 mM, respectively, and stored at -20°C in small aliquots. The treatment solutions were prepared by diluting the stock solutions directly into the embryo medium and kept at 28,5°C. All treatment concentrations of PD166866 and DMH1 were of 8 and 12 μM and were determined based on our previous study to have optimal inhibition effects with virtually no toxic effects (Haerlingen et al., 2019). As a control group, embryos were treated with 0,1% dimethyl sulfoxide (DMSO) for all treatment conditions. All solutions were supplemented with 0,01 mg/mL methylene blue to prevent bacterial growth and, if treatment runs until 24 hpf or later and if embryos are intended for whole mount *in situ* hybridization (WISH), with 0,003% 1-phenyl-2-thiourea (PTU).

Two hours before treatments, embryos were staged and stage-matching embryos were pooled and randomly allocated to the different experimental treatments into 60mm Petri dishes, 40-50 maximum per Petri dish. All abnormal or poorly developed embryos were excluded. Depending on the experiments and sampling stages, treatment periods included the following (in hpf): 10-13; 13-16; 16-19; 19-21, 21-24, 10-24; 10-14; 14-18; 18-22; 22-26; 10-22 and; 10-26. Treatment periods are indicated in the text and the corresponding figures. Treatments were always performed in duplicates. All embryos were also staged before starting and finishing the treatments to ensure correct timing. To start the treatments, the embryo media were entirely removed and replaced by 6 mL of the small molecule solutions and embryos were incubated at 28,5°C in the dark until the end of the treatment. Small molecule solutions were entirely removed, and embryos were washed three times with clean embryo medium, transferred into clean 96 mm Petri dishes, incubated for 10 minutes and, washed a fourth time with clean embryo medium. The new embryo media contained 0,01 mg/mL methylene blue if the treatment was stopped before 21 hpf and, 0,003% PTU if embryos were intended for WISH. Embryos were dechorionated and sampled as described above.

Heat-shock induction

For heat-shock experiments, Tg(*hsp70*:ca-fgfr1) and Tg(*hsp70*:*bmp2b*) were always out-crossed with either *AB (wild-type), Et(*nkx2.4b*:YFP), Tg(*myl7*:EGFP), Tg(*sox17*:EGPF), or with each other, depending on the experiments. Around 8/9 hpf, the Tg(*hsp70*:ca-fgfr1) and Tg(*hsp70*:*bmp2b*) embryos were staged and the stage-matching embryos from the different founders of the same transgenic line were pooled and randomly allocated to the different heat-shock times into 96 mm Petri dishes, maximum 80 embryos per dish. All abnormal or poorly developed embryos were excluded. Heat-shock stage included (in hpf): 10 (early segmentation);

15 (mid segmentation); 20 (late segmentation) and; 10, 15 and 20 (serial heat-shock/whole segmentation). All treatments were always performed in duplicates. For the heat-shocks, embryo media were entirely removed and replaced by embryo medium pre-heated at 40°C and embryos were incubated at 40°C for 30 minutes. After 30 minutes, warm media were entirely removed and replaced by normal temperature (28,5°C) embryo medium. The new embryo media contained 0,01 mg/mL methylene blue, and if embryos were intended for WISH, 0,003% PTU. Embryos were dechorionated and sampled as described above. For the heat-shocks applied during a small molecule treatment, the heat-shocks were performed as described here but warm (40°C) small molecule solution was used instead.

F0 CRISPR-Cas9-mediated pax2a knock-out

CRISPR-Cas9-mediated *pax2a* and *adamtsl2* knock-out were performed as previously described (Trubiroha et al., 2018) and summarized here. DNA templates for the *pax2a* and *adamtsl2* single-guide RNAs (sgRNAs) synthesis were produced by annealing a scaffold oligonucleotide (5'-AAAGCACCGACTCGGTGCCACTTTTTCAAGTTGATAACGGACTAGCCTTATTTTAACTTGCTATTTCTAGCTCTAAAAC-3') with an oligonucleotide which contains from 5' to 3': the SP6 promoter sequence, the gene-specific guide RNA target sequence (underlined in the sequence provided hereafter) and a segment of the complementary scaffold oligonucleotide sequence. Entire sequence for the (1) *pax2a* sgRNA: 5'-GCGATTTAGGTGACACTATA<u>GGCGGTGTGAACCAGCTAGG</u>GTTTTAGAGCTAGAAATAG-3'; (2) *adamtsl2* sgRNA 5'-GCGATTTAGGTGACACTATA<u>GGCTGGAAGTGATCACATAC</u>GTTTTAGAGCTAGAAATAG-3'. The gene-specific guide RNA target sequences were designed using the SSC software (H. Xu et al., 2015). PCR amplification was performed using the Taq PCR Core Kit (Qiagen) with 20 nM of each of the scaffold and gene-specific oligonucleotide and 260 nM of each of the universal flanking primer (forward: 5'-GCGATTTAGGTGACACTATA-3', reverse: 5'-AAAGCACCGACTCGGTGCCAC-3'). PCR products were purified using a standard phenol-chloroform-isoamylalchohol extraction.

sgRNA were synthetized using the SP6 RNA polymerase in a 20 μL reaction volume with 1 µg of purified DNA template, 1x SP6 reaction buffer (provided with the SP6 RNA polymerase), 2.5 mM of each rNTP, 40 U of RNase inhibitor, and 6 U of Large Fragment of DNA Polymerase I. Reaction mix was first incubated for 15 minutes at room temperature (RT) without the SP6 RNA-polymerase and then, the SP6 was added (20 U). After overnight (ON) incubation at 40°C,

3 U of DNAse I were added to the reaction mix and sgRNAs were purified using High Pure PCR Cleanup Micro Kit according to supplier's instructions. sgRNA quality was assessed on electrophoresis gel and concentration was measured.

Micro-injection mix was prepared with 80 ng/µL sgRNA, 100 ng/µL Cas9 protein, 200 mM KCl solution, and 0.15% phenol red and was incubated for 5 minutes at RT to allow the Cas9 protein to bind onto the sgRNA. 3 nL of this mix was micro-injected into 1-cell stage Et(*nkx2.4b*:YFP) embryos. Embryos were allowed to develop in standard conditions until sampling. In addition, non-injected embryos, *adamtsl2* sgRNA served as micro-injection control as we previously shown that this gene is expressed in the thyroid cells but *adamtsl2* crispants have no thyroid phenotype (Trubiroha et al., 2018). CRISPR-Cas9-mediated mutagenesis efficiency was assessed by the reduction in the Pax2a immunostaining signal and by PCR-based genotyping (see below). No stable mutant line was established.

Whole-mount immunofluorescence

Whole-mount immunofluorescence (WIF) was essentially performed as previously described (Opitz et al., 2011) and summarized here. After ON incubation in 4% PFA at 4°C, embryos were rinsed with PBS supplemented with 0,1% of Tween20 (PBST) and, processed into WIF within the next two days. Embryos were permeabilized by proteinase K incubation, whose features depended on the apparent developmental stage (see Table S1). Embryos were then stabilized with 4% PFA incubation for 25 minutes. Next, embryos were washed with PBST and incubated for 4-6 hours in PBST containing 10 mg/mL bovine serum albumin, 4% horse serum, 1% DMSO and 0,8% Triton X-100 (referred to as blocking PBST, bPBST) at RT under gentle shaking. bPBST was removed and replaced with primary antibodies-containing bPBST for ON incubation at 4°C. The next day, antibodies solutions were removed, and embryos were rinsed with PSBT and incubated ON at 4°C in secondary antibodies-containing bPBST. The third day, embryos were rinsed again with PBST. The following antibodies (and their dilution) were used: Pax2a (1:250); E-Cadherin (1:200); GFP (1:1000, also recognizes d2EGFP and YFP); rabbit monomeric destabilized Kusabira Orange 2 (dmKO2, 1:250); mouse dmKO2 (1:200); cy3-donkey anti-rabbit IgG (1:250); cy3-donkey anti-mouse IgG (1:250); Alexa Fluor 647-donkey anti-rabbit IgG (1:250); Alexa Fluor 647-donkey anti-mouse IgG (1:250); Alexa Fluor 488-goat anti-chicken IgG (1:250); Alexa Fluor 488-donkey anti-chicken IgG (1:250); Alexa Fluor 647-donkey anti-goat IgG (1:250) (see Key Resources Table for suppliers and references).

Single and dual-color whole-mount in situ hybridization

The whole-mount *in situ* hybridization protocol was largely based on the one published by Thisse and Thisse (C. Thisse and B. Thisse, 2008). Briefly, PFA solution was washed with RNAse-free (RF) PBST and embryos were gradually dehydrated through series of PBST baths containing increasing concentrations of methanol (25, 50, 75, 100%) and stored at -20°C until needed. Embryos were re-hydrated through series of PBST washes containing decreasing concentrations of methanol, permeabilized, and stabilized as described for the WIF procedure. Embryos were first shortly incubated in 45°C hybridization mix (HM) and then incubated for five hours in 65°C HM. After five hours, HM was replaced by riboprobes-containing HM (0,2 ng/μL) and embryos were incubated for at least 16 hours at 65°C. The next day, the riboprobe solutions were removed, collected, and replaced by 65°C HM with no yeast tRNA and no heparin. Note that until now, all materials and reagents had to be strictly RF. Embryos were washed with gradually more concentrated 65°C SSC solution and then in PBST. Embryos were incubated for five hours in PBST containing 2 mg/mL bovine serum albumin, 2% (v/v) sheep serum (referred to as sheep blocking PBST, sbPBST) and ON at 4°C in sbPBST containing alkaline phosphate (APh)-coupled anti-digoxigenin (DIG) (1:6000) or APh-coupled anti-dinitrophenyl (DNP) (1:500) antibodies, depending on the riboprobes. On the third day, embryos were washed with PBST and equilibrated in alkaline tris buffer (pH 9,5) for 1 hour. Blue stainings were performed using NBT/BCIP for the *tg* riboprobe or BM Purple for all other riboprobes. Staining was stopped with several PBST washes. In case of dual-color WISH, embryos were incubated for 10 minutes in PBST supplemented with 1% (w/v) glycine with pH adjusted to 2,2 with hydrochloric acid, washed with PBST and incubated a second time in sbPBST. Embryos were transferred into APh-coupled anti-fluorescein-containing (1:2000) sbPBST for ON incubation at 4°C. The staining procedure on the fourth day was the same than on the third day with the following differences: the alkaline buffer pH was 8,2 and the fluorescein-tagged riboprobe was revealed using FastRed according to supplier's instruction but dissolved in 0,5 M NaCl solution. Embryos were kept in 95% glycerol at 4°C for imaging and long-term storage. (Additional technical details and solution compositions can be found in C. Thisse and B. Thisse, 2008).

Riboprobe synthesis

Total mRNAs were extracted and purified using TissueRuptor and Qiagen RNeasy Mini Kit following supplier's instructions. The purified mRNAs were used as substrate for the SuperScript II reverse transcriptase to generate cDNA libraries. Gene-specific cDNAs were amplified by PCR, whose reverse primer contained on its 5' end the T3 RNA polymerase promoter sequence (5'-GGATCCATTAACCCTCACTAAAGGGAA-3') (see Key Resources Table). *myl7* riboprobe

template was obtain from linearized plasmid (Yelon et al., 1999). DNA templates were purified with the MinElute PCR Purification Kit according to supplier's instruction and a standard phenol-chloroform-isoamylalchohol extraction. PCR-generated templates were then incubated 15 minutes at RT with 10 mM DTT, RNAse OUT, DNA polymerase I-Klenow fragment, the T3 RNA polymerase buffer and the ribonucleoside triphosphate (rNTPs). For the DIG-tagged probes, a ready-to-use DIG RNA labelling mix was used whereas the rNTPs mix was made by us using normal rNTPs and DNP-11-UTP for the DNP-tagged *tg* riboprobe. T3 polymerase was added after the 15 minutes incubation, and the mixes were further incubated at 37°C for 150 minutes. Plasmid-based probes did not require DNA polymerase I-Klenow fragment treatment; T7 RNA polymerase was immediately added, and the mixture was incubated for 150 minutes at 37°C. The *myl7* riboprobe was tagged with the ready-to-use FLU RNA labelling mix. The DNA templates were digested by incubating the reaction mixes with 3U of RF DNAse I. Synthesized product was purified using High Pure PCR Cleanup Micro Kit following supplier's instructions. Riboprobes were stored at -80°C until use.

Image acquisition & cell counting

After WISH staining, embryos were imaged using a Leica DFC420C camera mounted on a Leica MZ16F stereomicroscope in 4°C 95% glycerol for whole-mount imaging. Cropped raw images are shown.

Whole mount embryos pictures of WIF were acquired using a Leica DFC7000T camera mounted on a Leica M165FC stereomicroscope. Embryos were embedded in 1% low melting agarose to maintain them perfectly steady. Cropped raw images are shown.

Before confocal imaging thyroid primordia were isolated. To do so, embryos were embedded in 7% low melting agarose for transverse, sagittal or, frontal sectioning (indicated in the figure legends) on a Leica VT1000S. All vibratome sections were transverse sections (unless if indicated otherwise) and measured 100 µm in thickness. Vibratome sections were mounted on custom-made #1.5 72x26 mm glass slides using Glycergel to allow dual-side confocal imaging. Sections were imaged using a Zeiss 510 meta confocal microscope with a 40x magnification. Images were processed on ImageJ/Fiji with a 1-pixel radius Minimum filter to remove secondary antibody aggregate artefacts. For cell counting, thyroid primordia considered as complete were image as a z-stack. Cell counting were performed manually on these z-stacks on Zeiss ZEN Blue.

All whole mount WISH and WIF and confocal images show embryos representative of the phenotype of interest.

Genotyping

Tg(*hsp70*:ca-fgfr1) embryos were genotyped by amplifying the mCherry transgene (forward primer: 5'-CTCCAAGGCCTACGTGAAGCAC-3'; reverse primer: 5'-CACGGGCTTCTTGGCCTTG-3') and Tg(*hsp70*:*bmp2b*) embryos by amplifying a segment overlapping on the *hsp70* promoter and the *bmp2b* coding sequence (forward primer: 5'-CATGTGGACTGCCTATGTTCATC-3'; reverse primer: 5'-GAGAGCGCGGACCACGGCGAC-3').

CRISPR-Cas9-mediated mutagenesis for *pax2a* and *adamtsl2* efficiency was qualitatively assessed by PCR amplification of a small region flanking the targeted site (primers: *pax2a* forward: 5'-TGTGTCTGTGTTGTTGTATCCC-3'; *pax2a* reverse: 5'-TGGCTGACCCGTAGTTGTCT-3'; *adamtsl2* forward: 5'-GCTTCAGACAGTGTCTCTCCTG-3'; *adamtsl2* reverse: 5'-GCTTCAGACAGTGTCTCTCCTG-3'). PCR products were analyzed by heteroduplex mobility assay, as previously described in our previous report (Trubiroha et al., 2018).

QUANTIFICATION AND STATISTICAL ANALYSIS

Sample sizes are always indicated on the figure or in its legend. On cell counting graphs, each dot represents data from a single embryo, unless it is indicated otherwise.

Statistical significances were calculated with an unpaired parametric t-test with a Welch's correction and a two-tailed p value (95%) on Prism7. The bars in the cell counting plots always represent the means.

"Normal thyroid", "Reduced size and/or staining intensity" and "Increased size/or staining intensity" categories were determined visually. When genotyping was performed, all analyses were done blinded to the embryos' genotype.

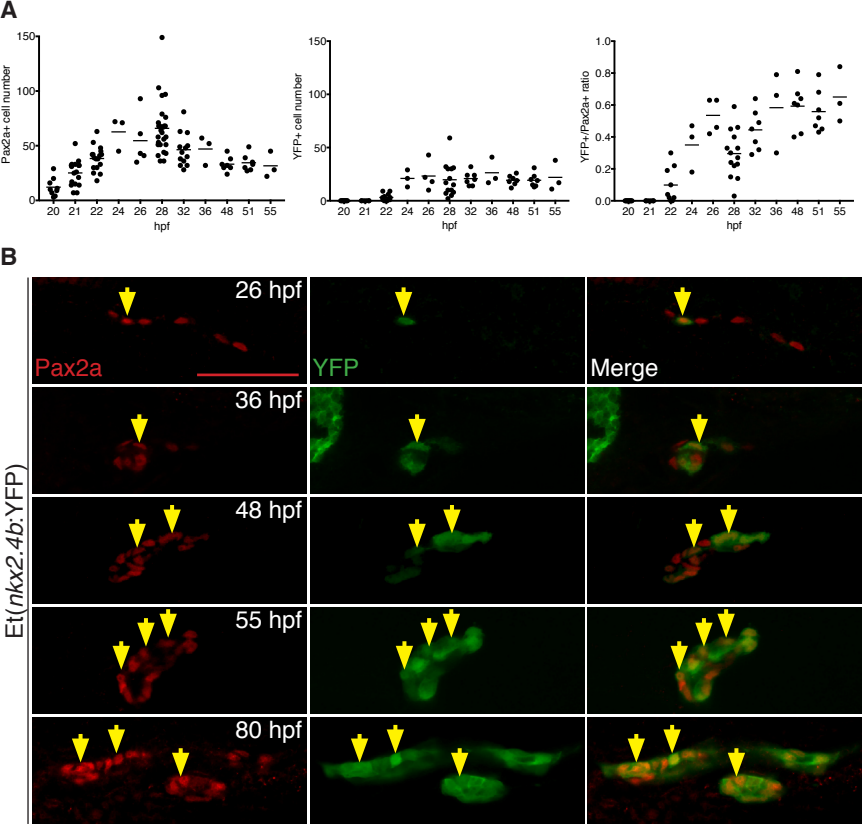
A
Pax2a+ cell number
YFP+ cell number
YFP+/Pax2a+ ratio
hpf
20 21 22 24 26 28 32 36 48 51 55
B
Et(nkx2.4b:YFP)
26 hpf
36 hpf
48 hpf
55 hpf
80 hpf
Pax2a
YFP
Merge

Fig. 1

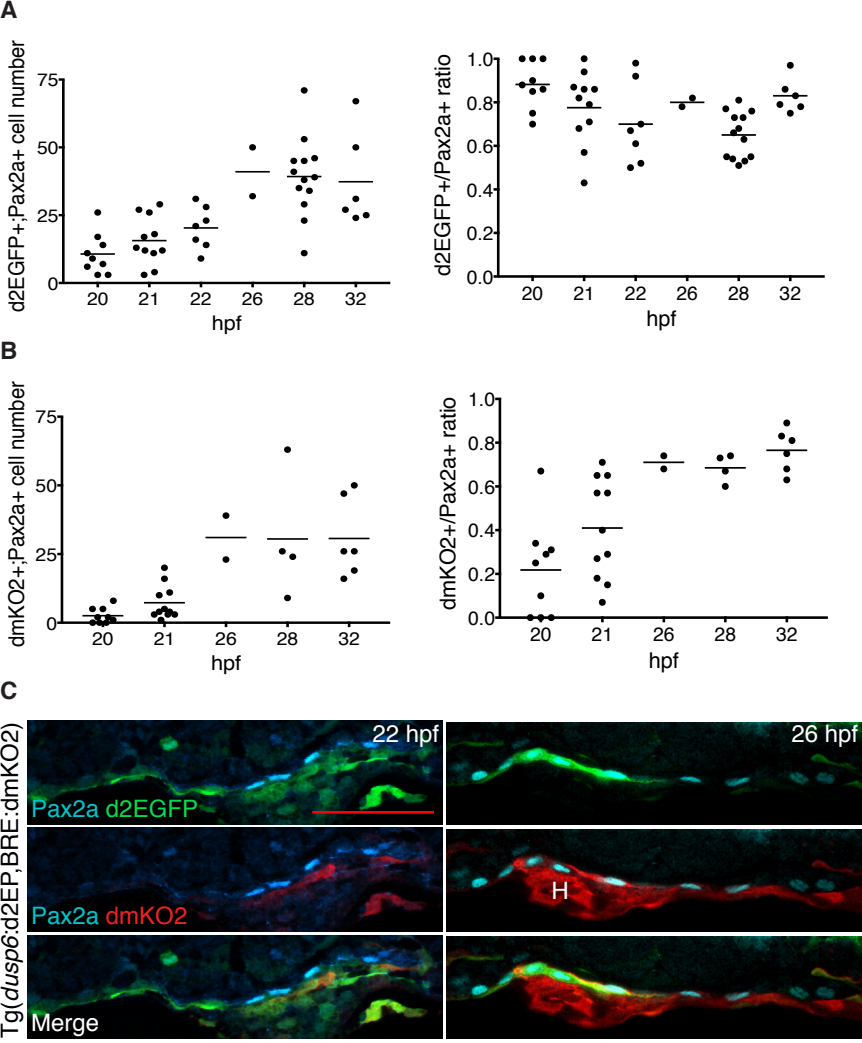
A
d2EGFP+;Pax2a+ cell number
75
50
25
0
20
21
22
26
28
32
hpf
d2EGFP+/Pax2a+ ratio
1.0
0.8
0.6
0.4
0.2
0.0
20
21
22
26
28
32
hpf
B
dmKO2+;Pax2a+ cell number
75
50
25
0
20
21
26
28
32
hpf
dmKO2+/Pax2a+ ratio
1.0
0.8
0.6
0.4
0.2
0.0
20
21
26
28
32
hpf
C
Tg(dusp6:d2EP,BRE:dmKO2)
22 hpf
26 hpf
Pax2a d2EGFP
Pax2a dmKO2
H
Merge

Fig. 2

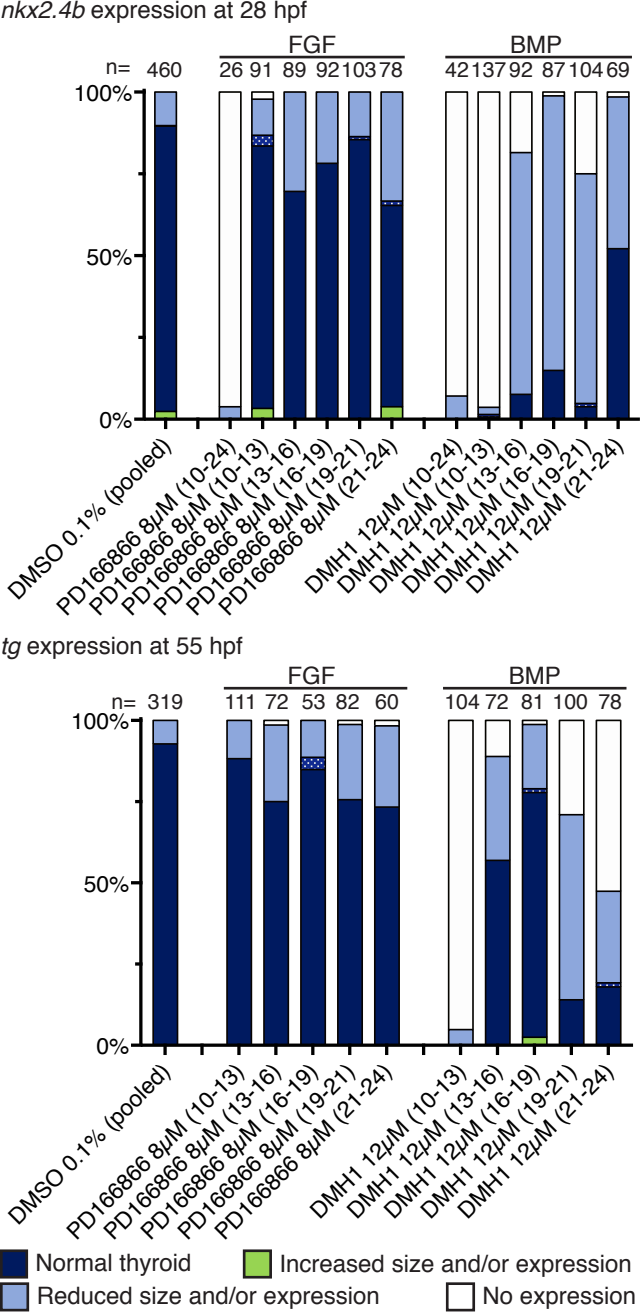
nkx2.4b expression at 28 hpf
FGF
BMP
n= 460
26 91 89 92 103 78
42 137 92 87 104 69
100%
50%
0%
DMSO 0.1% (pooled)
PD166866 8μM (10-24)
PD166866 8μM (10-13)
PD166866 8μM (13-16)
PD166866 8μM (16-19)
PD166866 8μM (19-21)
PD166866 8μM (21-24)
DMH1 12μM (10-24)
DMH1 12μM (10-13)
DMH1 12μM (13-16)
DMH1 12μM (16-19)
DMH1 12μM (19-21)
DMH1 12μM (21-24)
tg expression at 55 hpf
FGF
BMP
n= 319
111 72 53 82 60
104 72 81 100 78
100%
50%
0%
DMSO 0.1% (pooled)
PD166866 8μM (10-13)
PD166866 8μM (13-16)
PD166866 8μM (16-19)
PD166866 8μM (19-21)
PD166866 8μM (21-24)
DMH1 12μM (10-13)
DMH1 12μM (13-16)
DMH1 12μM (16-19)
DMH1 12μM (19-21)
DMH1 12μM (21-24)
Normal thyroid
Increased size and/or expression
Reduced size and/or expression
No expression

Fig. 3

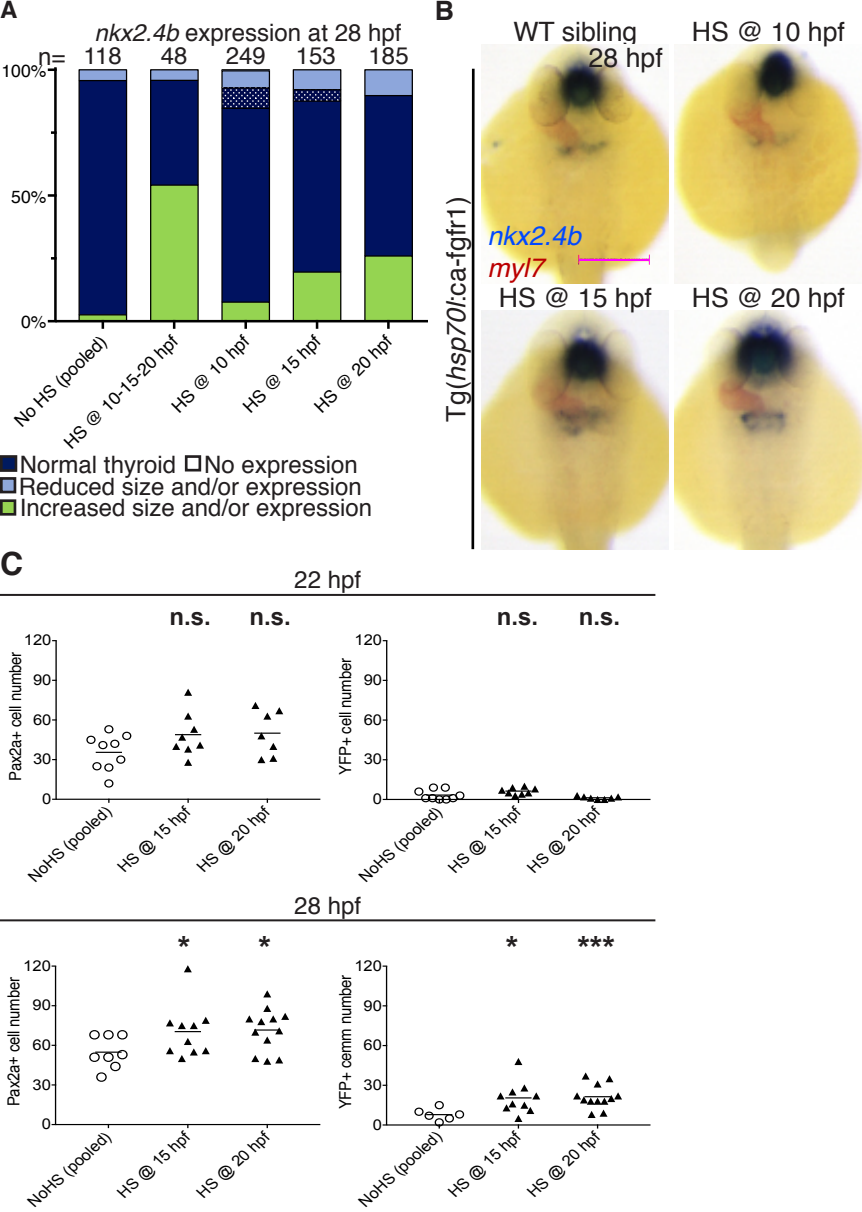
A
nkx2.4b expression at 28 hpf
n= 118 48 249 153 185
100%
50%
0%
No HS (pooled)
HS @ 10-15-20 hpf
HS @ 10 hpf
HS @ 15 hpf
HS @ 20 hpf
Normal thyroid
No expression
Reduced size and/or expression
Increased size and/or expression
B
WT sibling
28 hpf
HS @ 10 hpf
nkx2.4b
myl7
HS @ 15 hpf
HS @ 20 hpf
Tg(hsp70l:ca-fgfr1)
C
22 hpf
n.s.
n.s.
Pax2a+ cell number
YFP+ cell number
NoHS (pooled)
HS @ 15 hpf
HS @ 20 hpf
28 hpf
*
***
YFP+ cemm number

Fig. 4 (v2)

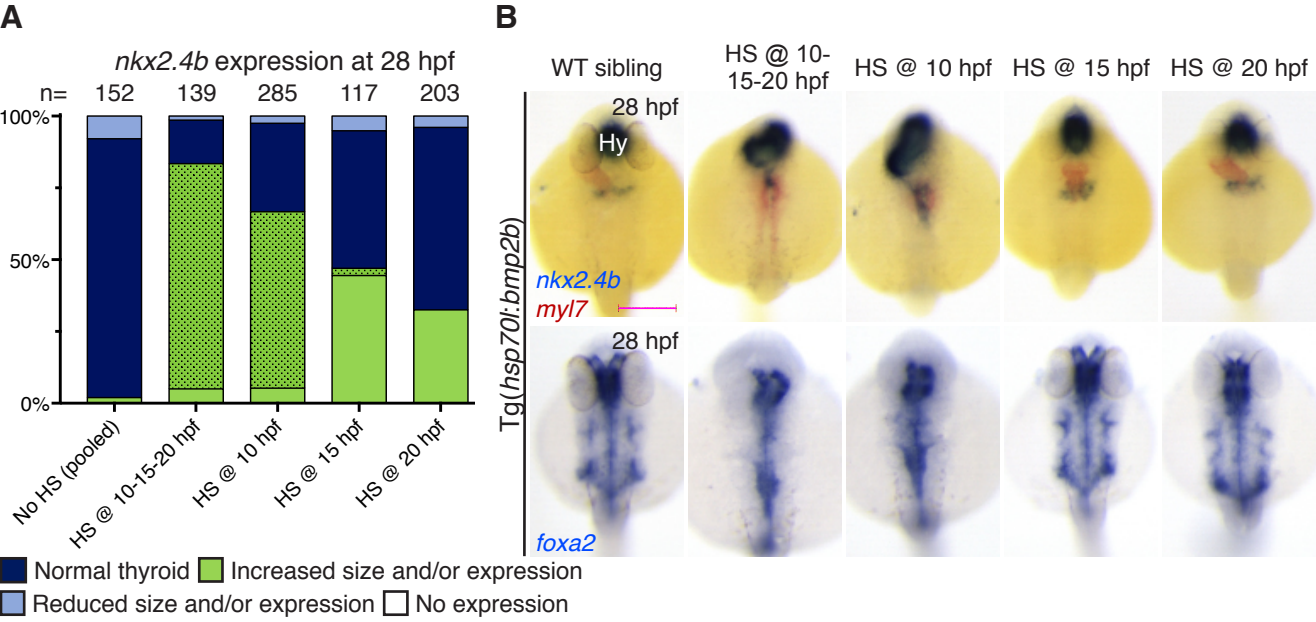
A
nkx2.4b expression at 28 hpf
n= 152 139 285 117 203
100%
50%
0%
No HS (pooled)
HS @ 10-15-20 hpf
HS @ 10 hpf
HS @ 15 hpf
HS @ 20 hpf
Normal thyroid
Increased size and/or expression
Reduced size and/or expression
No expression
B
WT sibling
HS @ 10-15-20 hpf
HS @ 10 hpf
HS @ 15 hpf
HS @ 20 hpf
Tg(hsp70l:bmp2b)
28 hpf
Hy
nkx2.4b
myl7
28 hpf
foxa2

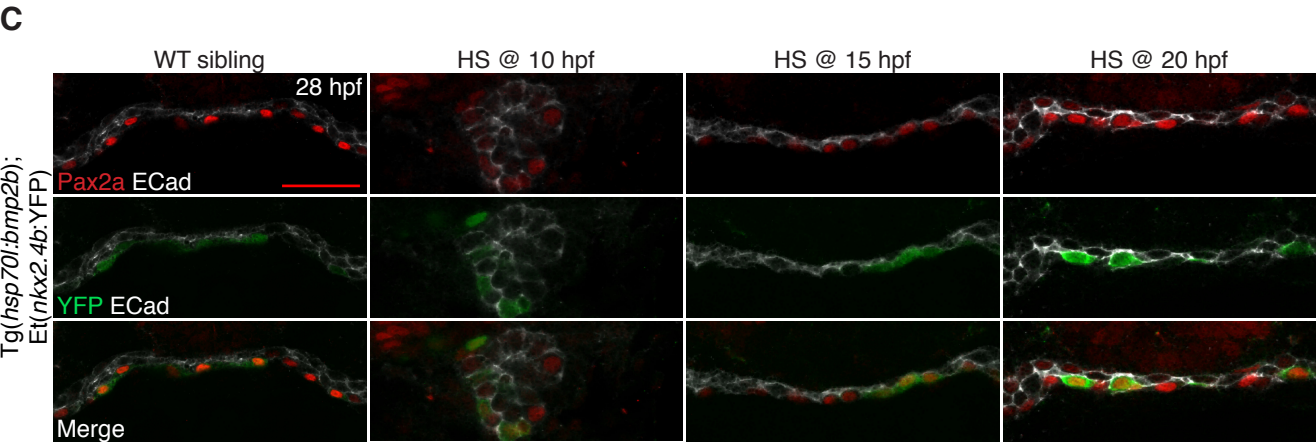
C
WT sibling
HS @ 10 hpf
HS @ 15 hpf
HS @ 20 hpf
Tg(hsp70l:bmp2b); Et(nkx2.4b:YFP)
28 hpf
Pax2a ECad
YFP ECad
Merge

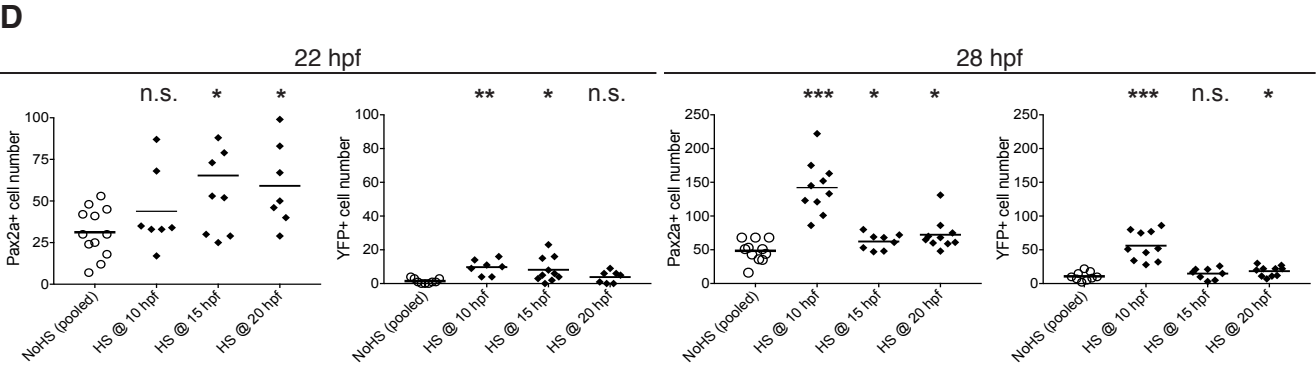
D
22 hpf
28 hpf
Pax2a+ cell number
YFP+ cell number
n.s. * *
** * n.s.
*** * *
*** n.s. *
NoHS (pooled)
HS @ 10 hpf
HS @ 15 hpf
HS @ 20 hpf

Fig. 5

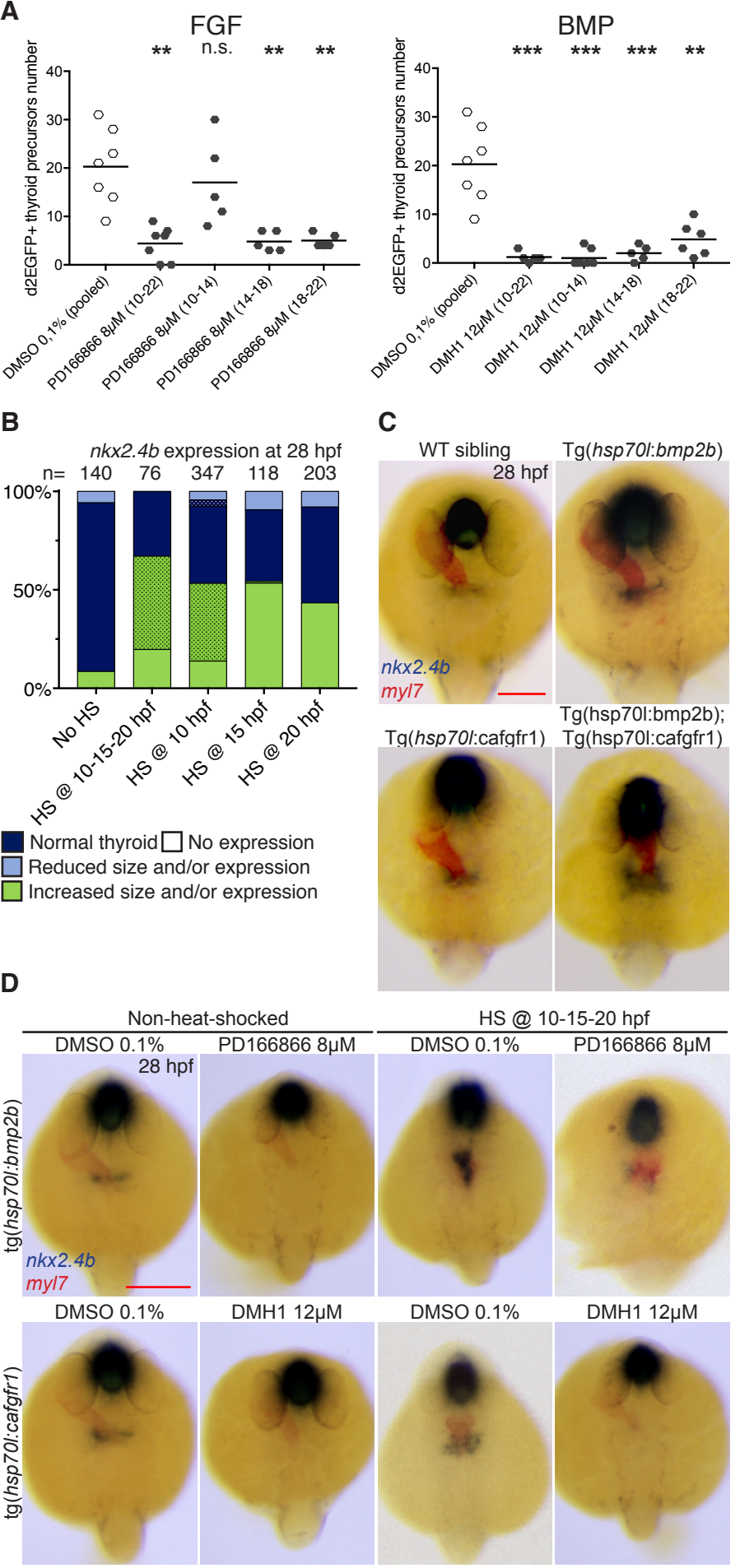
A
FGF
BMP
d2EGFP+ thyroid precursors number
**
n.s.
**
**
***
***
***
**
DMSO 0,1% (pooled)
PD166866 8μM (10-22)
PD166866 8μM (10-14)
PD166866 8μM (14-18)
PD166866 8μM (18-22)
DMH1 12μM (10-22)
DMH1 12μM (10-14)
DMH1 12μM (14-18)
DMH1 12μM (18-22)
B
nkx2.4b expression at 28 hpf
n= 140 76 347 118 203
100%
50%
0%
No HS
HS @ 10-15-20 hpf
HS @ 10 hpf
HS @ 15 hpf
HS @ 20 hpf
Normal thyroid
No expression
Reduced size and/or expression
Increased size and/or expression
C
WT sibling
Tg(hsp70l:bmp2b)
28 hpf
nkx2.4b
myl7
Tg(hsp70l:cafgfr1)
Tg(hsp70l:bmp2b);
Tg(hsp70l:cafgfr1)
D
Non-heat-shocked
HS @ 10-15-20 hpf
DMSO 0.1%
PD166866 8μM
DMSO 0.1%
PD166866 8μM
28 hpf
tg(hsp70l:bmp2b)
nkx2.4b
myl7
DMSO 0.1%
DMH1 12μM
DMSO 0.1%
DMH1 12μM
tg(hsp70l:cafgfr1)

Fig. 6

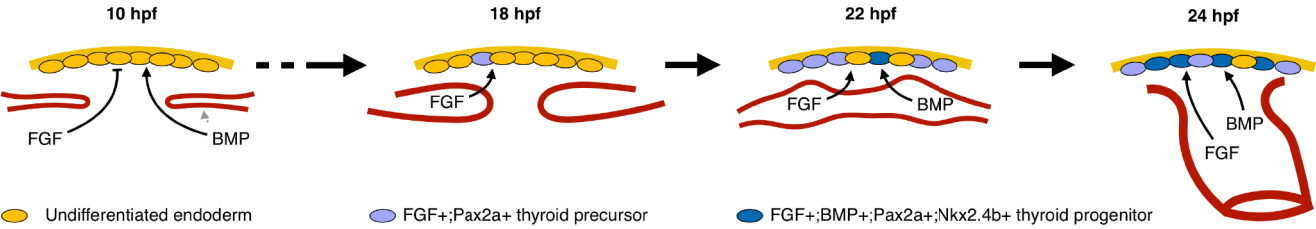
10 hpf
18 hpf
22 hpf
24 hpf
FGF
BMP
FGF
FGF
BMP
BMP
FGF
Undifferentiated endoderm
FGF+;Pax2a+ thyroid precursor
FGF+;BMP+;Pax2a+;Nkx2.4b+ thyroid progenitor

Fig. 7